5-2012

A Survey of Mission Opportunities to Trans-Neptunian Objects – Part II

Ashley M. Gleaves
University of Tennessee - Knoxville, agleaves@utk.edu

A Survey of Mission Opportunities to Trans-Neptunian Objects – Part II

Ashley Gleaves[Σ], Randall Allen[Σ], Adam Tupis[Σ], John Quigley[Σ], Adam Moon[Σ], Eric Roe[Σ], David Spencer[Σ], Nicholas Youst[Σ], and James Evans Lyne[Π]

The University of Tennessee, Knoxville, TN, 37916

The design of high thrust missions to seven trans-Neptunian objects are discussed. Final targets include Huya, Ixion, Orcus, Rhadamanthus, Salacia, Sedna, and Varuna. Launch opportunities were optimized for minimum C3 and low arrival velocity to maximum the options available upon arrival. All trajectories use a gravity assist flyby at Jupiter with distances from 1.1 Jovian radii to over 20 radii. Missions were evaluated for durations of 25 or fewer years, with extended flight times leading to a decreased arrival velocity. For alternative transit methods, low thrust trajectories were found for a select target to determine the benefits and disadvantages as compared to high thrust. Radiation factors were also explored, but without conclusive results. Project results indicate that optimum flight times are approaching as soon as 2027 for launch to a TNO with the option of orbital insertion, with many opportunities following.

Nomenclature

A	= Amplitude
a	= Semi-Major Axis
B	= Offset Distance
b	= Semi-Minor Axis
C	= Coefficient
E	= Energy
e	= Eccentricity
I_{sp}	= Specific Impulse
i	= Inclination
m	= Mass
R, r	= Radius
V	= Velocity
ΔV	= Change in Velocity
δ	= Turn Angle
μ	= Gravitational Parameter
f	= Flyby
i	= Impact
LP	= Launch Payload
P	= Projectile
p	= Periapse
∞	= Hyperbolic Excess

I. Introduction

Launched in 2006, New Horizons was the first, and currently only, spacecraft launched with the intention of researching trans-Neptunian objects. The recent discovery of a large number of these TNOs of all orbits, sizes, and apparent compositions makes these bodies particularly intriguing. Since the orbits of TNOs fall so far away

[Σ] Undergraduate, Department of Mechanical, Aerospace, and Biomedical Engineering

[Π] Associate Professor and corresponding author. 414 Dougherty Building, The University of Tennessee at Knoxville, 37996. jelyne@utk.edu.

from the Earth's orbit, very little is known rather than speculated. Since TNOs are so varied, they have the potential to offer very unique insight into the formation and history of the solar system. The missions developed in this project were based on confirming suspected qualities of select TNOs, or discovering new and unexpected findings. A previous design group studied the TNOs Haumea, Makemake, Quaoar, and Sedna, and achieved very valuable results for future projects[1]. For this project, Huya, Ixion, Logos, Orcus, Rhadamanthus, Salacia, and Varuna were selected as targets, although later Logos was replaced with the previously examined Sedna for more in depth evaluation.

For each of the seven targets, the Atlas V 551 and Delta IV HLV were analyzed as the launch vehicle, launch windows were comprised based on the orbital period of Jupiter, and the arrival excess speed was used to evaluate arrival maneuver options. High thrust interplanetary trajectories were found for each target and per results of the previous group's research, each trajectory uses an unpowered Jupiter flyby. Since the launches are based on the availability of Jupiter for a flyby en route to a TNO, launch opportunities for a given target are roughly twelve years apart. In the interest of extra mission opportunities, a mission can typically be done the year before and the year after the optimum twelve year period. The intense radiation emitted by Jupiter prompted radiation analysis; this was done based on individual flight paths and is heavily based on the periapsis radius at Jupiter. Generally, the excess speed combined with extremely low gravitational parameters made an orbital mission impossible or impractical with current technology, although a few cases proved promising. Arrival options were then selected based on the orbital potential or physical information desired for the specific TNO. Additionally, low thrust options were explored as an alternative method for reaching the TNOs in hopes of lowing the required launch energy. To enhance the relevancy of results, radiation analysis was done to determine the need for and intensity of shielding for a given mission. The results found in this study are very promising for the possibility and practicality of a mission to a trans-Neptunian orbit for significant scientific advancement.

II. Launch

Two rockets for the initial launch were evaluated throughout the study, the Atlas V 551 and the Delta IV HLV. Their launch capabilities are shown in Figure 1. The mass capabilities for a specific launch energy, C3, were determined using a fifth order polynomial to fit the launch curves in Fig. 1. Equation (1) shows the polynomial with its coefficients following in Table 1 and was provided in Launching Science[2]. Figure 2 was made using Eq. (1) and shows the payload values in kilograms.

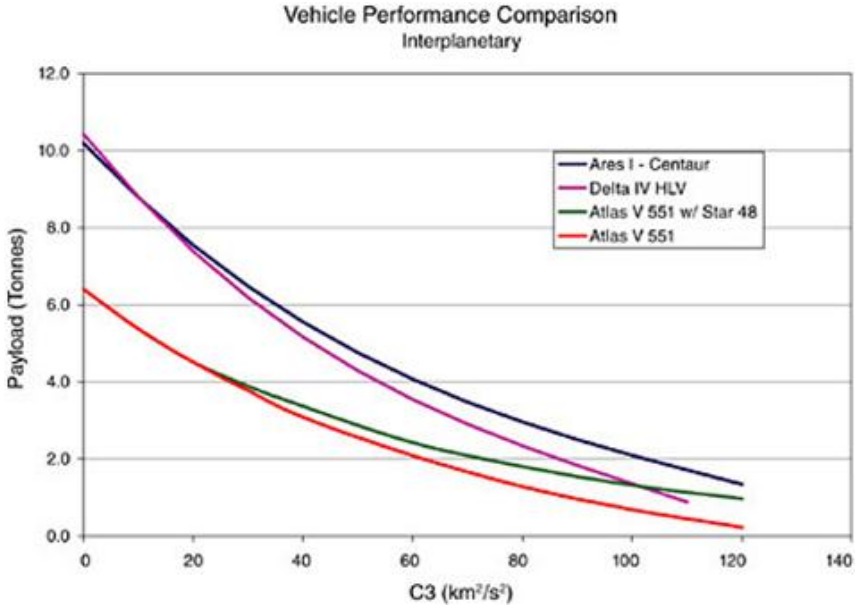

Figure 1. Payload vs C3. *From Launching Science, Figure 1 is a comparison of the payload capabilities of four rocket configurations as a function of C3.*

$$m_{LP} = C_0 + C_1 * C3 + C_2 * C3^2 + C_3 * C3^3 + C_4 * C3^4 \quad (1)$$

Table 1. Equation 1 coefficients. *Coefficients are listed for Equation 1 as applicable to the Atlas V 551 with Star 48B and Delta IV HLV. Maximum range valid and error are also included.*

Launch Vehicle	C_0	C_1	C_2	C_3	C_4	Max Range, C3	Error, kg
Atlas V551 with Star48B	$6.536*10^{3}$	-112.72	1.0171	$-5.2*10^{-3}$	$1.14*10^{-5}$	154	31.081
Delta IV HLV	$1.040*10^{4}$	-170.07	1.1109	$-2.7*10^{-3}$	$-5.00*10^{-6}$	98.84	26.981

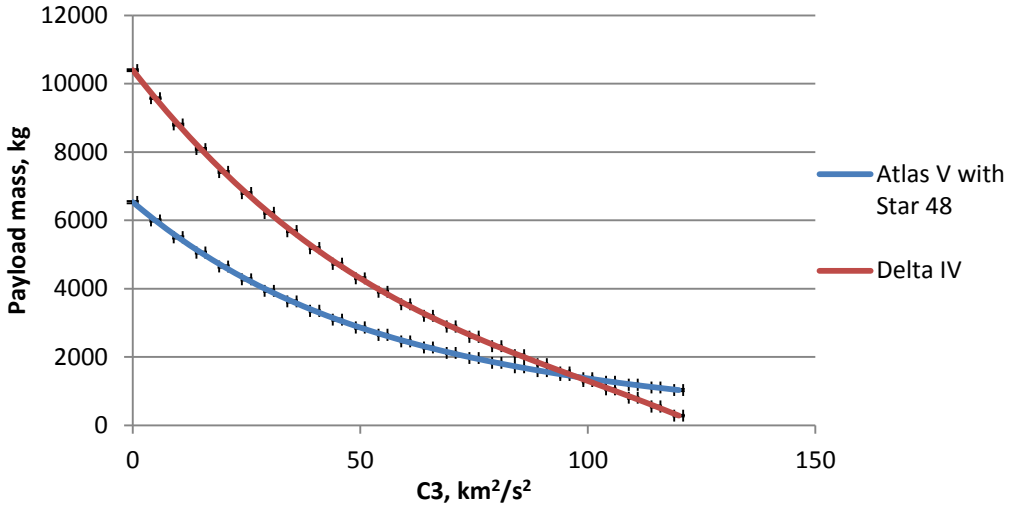

Figure 2. C3 vs Payload Mass. *Based on Fig. 1 and using Eq. 1, Fig. 2 shows the payload values in mass.*

Also listed in Table 1 are the error margins, which are included on Fig. 2. It should be noted that this polynomial method is accurate for the AtlasV 551 with Star48B within 31 kg and within 27 kg for the Delta IV HLV. The range of C3s the polynomial is valid for is 158 for the Altas V 551 with Star48B and 98 for the Delta IV HLV. The Delta IV HLV is evaluated for C3s out of this method's range, but the values do remain close to the maximum limit. The Delta IV HLV performs better at lower C3s where the curves can be considered acceptably accurate. In later figures, data for the Atlas V 551 with Star48B and the Delta IV HLV are displayed for easy comparison, but the data may be in a high C3 range where it is considered inaccurate for the Delta IV HLV. Certain missions may require more in depth analysis of launch capabilities, but for the purpose of this study, the above method was used. Basic launch mass capabilities as related to flight time are shown in Figure 3, with low flight time corresponding to high C3. As discussed above, the Delta IV HLV shows better performance for low C3s and high flight times, and the Atlas V 551 with Star48B performs better for high C3s and low flight times.

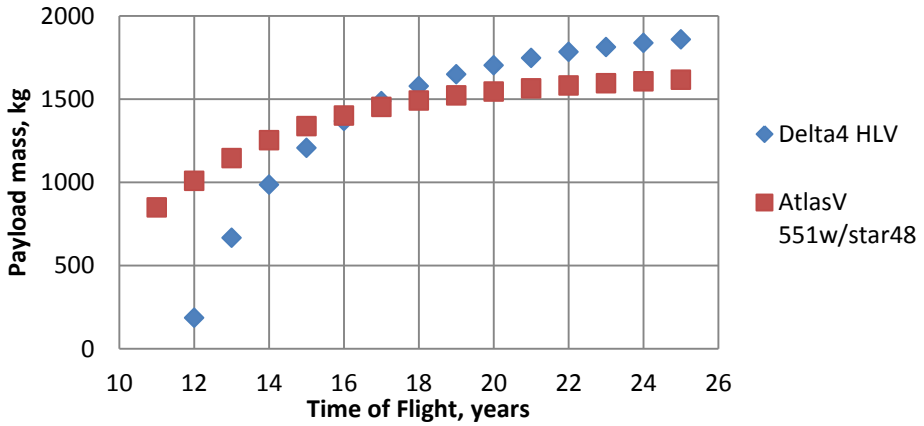

Figure 3. Payload Mass vs Time of Flight. *Payload capabilities at launch for the Delta IV HLV and AtlasV 551 with Star48B in relation to time of flight.*

Payload mass is assumed to be similar to that of New Horizons. The total weight of New Horizons was 478 kg, including a scientific payload of 30.4 kg[3]. The radioisotope thermoelectric generator used on New Horizons, GPHS RTG, has been replaced with a new RTG, the multi-mission RTG. The MMRTG is 14 kg less than the GPHS RTG, which allows for extra scientific payload assuming remaining masses are the same. Mission goals, such as determining density and mapping the surface, for the selected TNOs are very similar to that of New Horizons; therefore, assuming similar payload mass is acceptable. The following table is a mass breakdown of the equipment onboard New Horizons. Similar equipment is expected to be present on TNO missions. Pending launch energy, more equipment can be added.

Table 2. Scientific Equipment Expected for Missions.

Equipment Function	Mass, kg
Ultraviolet Imaging Spectrometer	4.5
Multispectral Visible Imaging Camera/ Linear Etalon Imaging Spectral Array	10.3
Radio Science Experiment	0.1
Long Range Reconnaissance Imager	8.8
Solar Wind Instrument	3.3
Energetic Particle Spectrometer	1.5
Dust Counter	1.9

III. General Methodology for Missions

The driving factor for finding appropriate launch dates was the orbital period of Jupiter. This period occurs roughly every twelve years, when Jupiter aligns properly with the TNO of interest for a flyby, and with Earth for low energy launch. Launch dates were evaluated spanning from 2022 to 2055, with each target having approximately three sets of launch dates falling in that time span. Also to be noted and evident in the trajectories, the majority of the TNOs are moving towards their apoapsis. This is shown in the increasing launch energies required the later a launch is planned. Given that the orbital period of Neptune is 164 years, waiting for an optimum launch date is not possible for bodies going in 'the wrong direction' with highly eccentric orbits. The longer a mission is not carried out, the closer humanity comes to losing an opportunity to explore a given TNO.

There were several constraints placed on the missions to increase launch practicality. The first constraint was that the lengths of planned missions were restricted to 25 years. This was done in the interest of timeliness and insurable technology life span. Secondly, according to the launch data, C3 was restricted to 120. Additionally, since all the trajectories use a Jupiter gravity assist flyby, JGA, the distance to Jupiter was kept above 1.1 Jovian radii from the planet in order to protect the spacecraft from unnecessary radiation hazards. These restraints combined with extensive tradeoff scenarios led to the ideal dates for launch opportunities.

During the actual trajectory development process, using trial and error, a reference date would be selected. Once a reference date was found, a variety of parameters were adjusted to find an acceptable launch date for a given target. Parameters adjusted were the launch date itself, mission duration, and Jupiter flyby date with an effort to minimize C3. A clear correlation between decreased mission duration and increased arrival excess speed can be seen in the results. This proves problematic because the gravitational parameters for the selected TNOs are incredibly small, requiring the change in speed to enter an orbit to be essentially the excess speed on arrival. Being able to enter an orbit at a TNO is ideal because this allows the surface of the body to be mapped. This allows very distinctive characteristics to be exposed and studied. By remaining at the TNO for the lifespan of the spacecraft, the composition, density, size, and mass can be discovered, either confirming or refuting current information. Learning the true size or composition of one TNO could even lead to being able to accurately describe other bodies with similar characteristics. Orbiting also allows for the observation of near-by bodies or of any satellites that may be present for a given TNO. The low gravitation parameters and high arrival speeds lead to the consideration of alternatives to orbiting. Flybys and impacts were considered and explored as other possibilities. Through the course of the project, it was decided that if orbiting was not possible, the arrival option that would provide the second largest collection of data was the impact mission. Extensive research was put into developing an appropriate method for impact.

Several software programs aided mission evaluation. Trajectories were found using Spaceflight Solutions's Mission Analysis Environment software, MAnE[4]. This was supplemented using Celestia[5] as a visual reference for the location of TNOs, although not every target was available. These two programs allowed for quick and relatively

easy selection of initial launch date guesses, and rapidly converged on ideal dates. All parameters reviewed were held or varied using MAnE and were easily compared or altered. Also extremely beneficial was the visual trajectory output, allowing for quick evaluation and adjustment based on the shape of the trajectory. MAnE was set to optimize for minimal C3 for a set of given parameters in order to have a specific focus for all missions. In addition to MAnE, arrival possibilities were evaluated using custom MATlab codes, focusing mainly on the ΔV required to orbit. A complete mission analysis covering C3, R_f and V_∞ evaluated for a single synodic period for Salacia using the above method follows for an orbital insertion. Complete trajectory data including the following and complete graphical detail for three synodic periods of each TNO target can be found in Reference 6.

A. Orbital Insertion

As mentioned above, the correlation between V_∞ and flight time play a vital role in the ability to orbit a given TNO, and are directly related. Also influential is the energy gained from a JGA and the initial launch energy. In order to gain an understanding of the relationship between these, Figure 4 was made for each TNO.

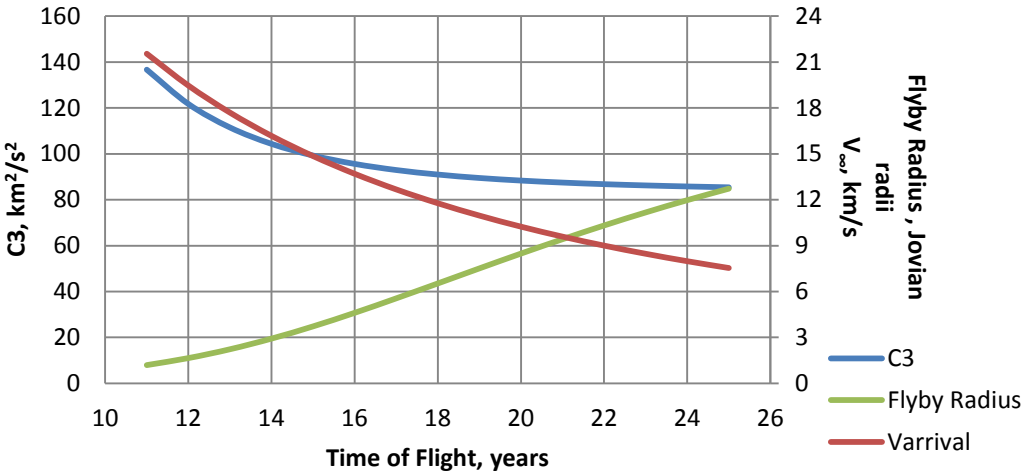

Figure 4. C3, Flyby Radius, V_∞ vs Time of Flight. *Figure shows the data for a launch to Salacia on 26 February 2043*

Once an optimum launch date was selected, a launch window was created to account delays, such as ill weather on the selected launch day or mechanical malfunctions. As expected, the C3 slowly increased as the dates were altered, although it had little effect on V_∞ and the flyby radius. This trend is shown in Figure 5. For Fig. 5, the JGA date was held constant in the interest of achieving the maximum benefit from a flyby regardless of launch date.

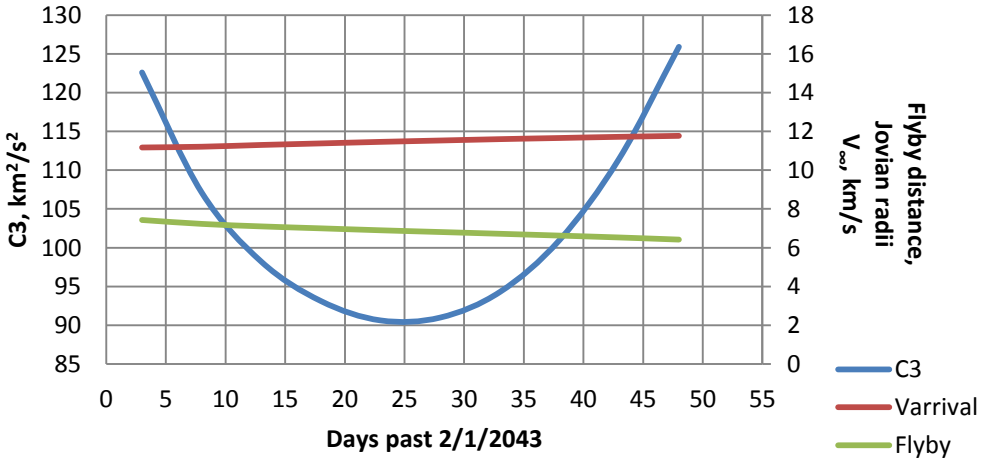

Figure 5. C3, Flyby Radius, V_∞ vs Launch Date. *Figure 5 shows the effect of varying the launch date with an initial date of 1 February 2043 for a Salacia mission.*

The launch energy directly relates to the cost of the mission and the additional payload that can be on board. The lowest C3 possible is ideal both in the interest of affordability and maximum scientific payoff. Although launch is possible with a C3 under 120 for approximately 20 days before or after the ideal launch date, the cost is great. To illustrate scientific losses, Figure 6 shows the difference in payload for the launch window in Fig. 5. The maximum mass is at the optimum launch date, and it drops by about a half at each end of the launch window. Not only does this affect the scientific equipment, but also the ability to carry an extra rocket for orbital insertion.

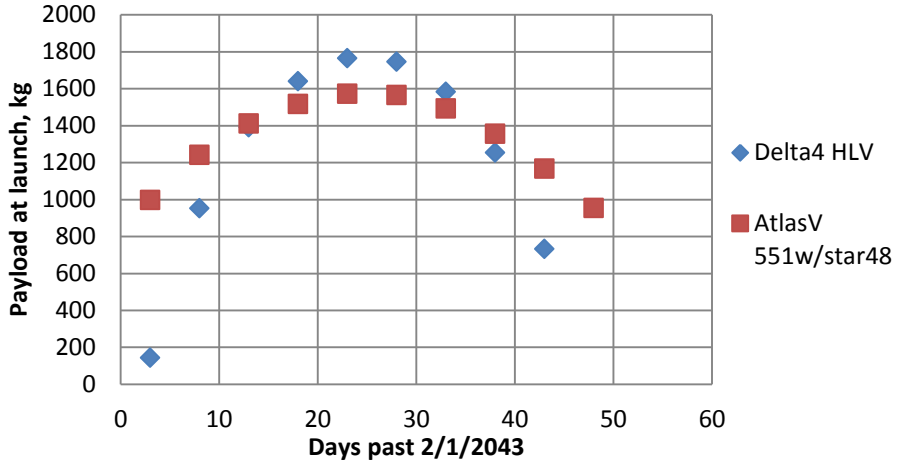

Figure 6. Payload at launch in relation to launch window. *Variation of payload according to launch date, shown for a mission to Salacia with a reference date of 1 February 2043.*

A dual stage rocket was found to be the most efficient method for TNO orbital insertion in terms of mass at launch and ΔV capabilities. Due to the smaller masses of the selected TNOs, the total V_∞ will have to be counteracted to slow the probe down enough for orbital insertion. In light of this, the ΔV required to orbit will for this analysis be equal to the V_∞ for a given target. A circular orbit is used to orbit all TNOs due to the fact the difference in a circular orbit and highly elliptical orbit in terms of velocity at periapse is negligible. Figure 7 below shows the ΔV capabilities of various rocket combinations and their masses fully loaded with propellant. Table 3 is the catalog system used to describe specific rocket combinations. All rockets and rocket information used were found in the May 2008 ATK Space Propulsion Products catalogue from Alliant Techsystems, Inc.[7].

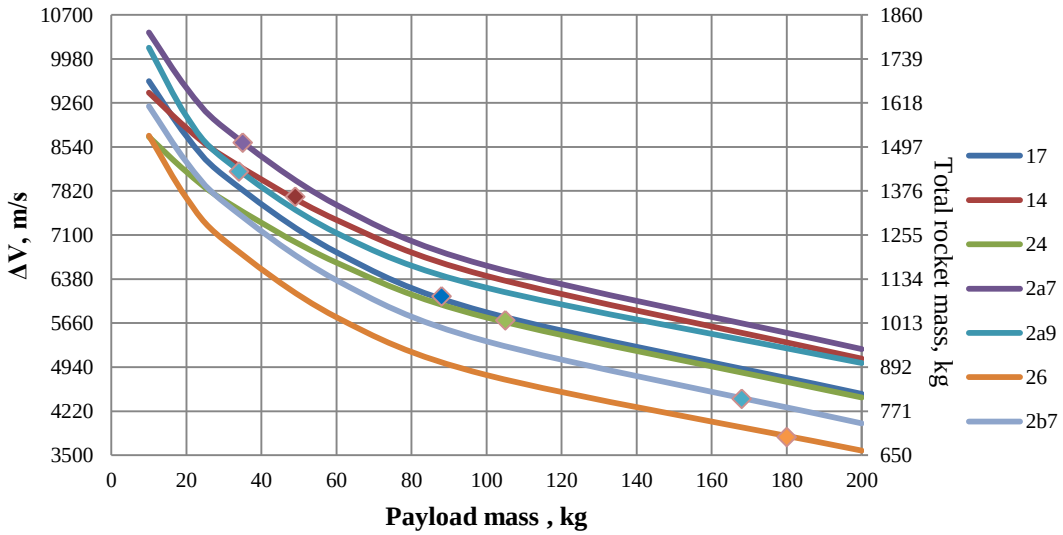

Figure 7. ΔV vs Payload for rocket combinations. *Rocket combinations are designated according to Table 3. The mass of each rocket combination along with its propellant mass is also plotted as the individual point placed along the curve of each rocket combination*

Table 3. Reference table for rocket combination numbers.
The reference number represents a specific ATK rocket, these are used to designate combination on the Figures 6, 7, and 8.

Reference number	ATK STAR designation	Total Rocket mass (kg)
1	37xfp	960.53
2	37N	620.9
2a	31	1382.7
2b	30e	678.9
3	30bp	543.1
4	27h	399.8
4a	24a	194.2
5	24c	238.6
5a	20a	314.0
6	17	79.1
7	17A	126.1
8	15g	93.7
9	13b	46.9
9a	13a	38.1

As the time of flight is increased, the ΔV necessary to orbit decreases due to the decreased V_∞. This trend is illustrated in Figure 8 which also illustrates the excess mass available for missions to Salacia in 2043 corresponding to varying time of flight. The excess mass is the payload in addition to the insertable mass, along with the rocket and its propellant for insertion for various rocket combinations and times of flight. Figure 8 uses a Delta 4 HLV and for comparison, the same is done using the Atlas V 551 rocket with a Star48B upper stage shown in Figure 9.

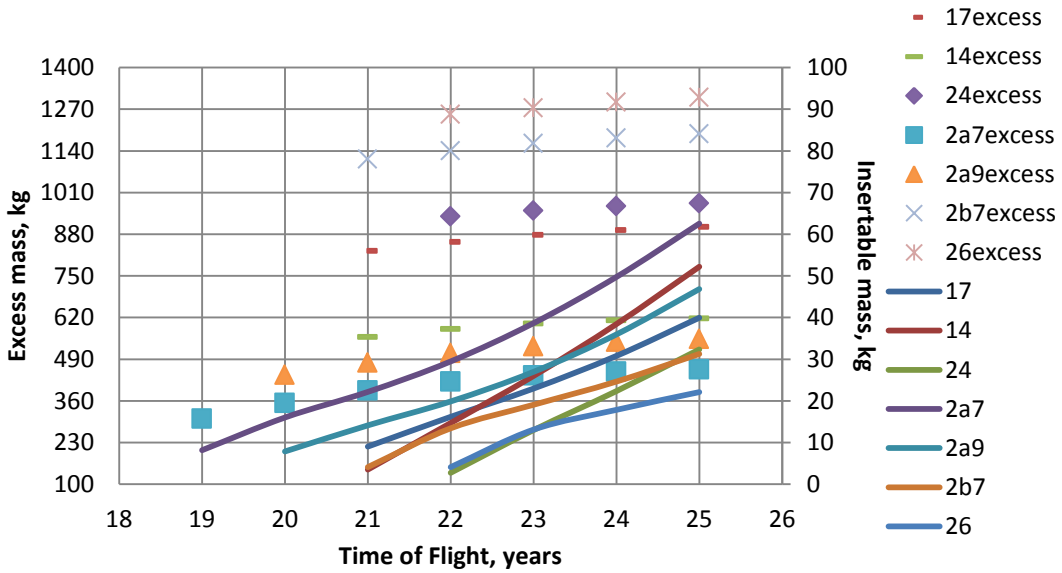

Figure 8. Insertable and Excess mass vs Time of Flight. *Insertable and excess mass for 2043 missions to Salacia corresponding to time of flight. The solid lines are insertable mass for each rocket combination and a specific time of flight; while the data points are the data for excess mass, using the Delta4 HLV launch vehicle, as a function of time of flight.*

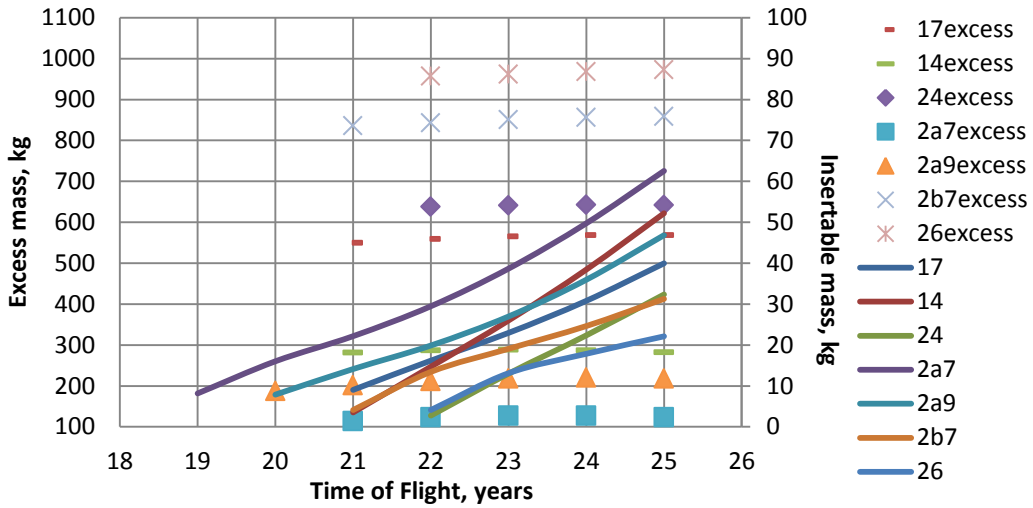

Figure 9. Insertable and Excess mass vs Time of Flight. *Excess and insertable mass capabilities using the AtlasV 551 with star48 for launch and various rocket combinations for orbital insertion. The solid lines are insertable mass while the individual points are excess mass. Both are dependant on time of flight, which is directly related to launch energy.*

Figures 8 and 9 show that the Delta IV HLV would be the preferred launch vehicle if launched with intent to orbit, and consequently with a low C3. This was predicted by the launch data.

B. Impact Mission Evaluation

Impact missions involve impacting the target TNOs with a projectile to collect information on the composition, mass, and density of the targets—an important objective when visiting a TNO. The following is based on the Deep Impact mission to the comet 9P/Tempel in 2005. An impactor will crash into the TNO's surface, generating a debris cloud and an impact crater. A flyby spacecraft will then collect data on the impact.

The first step in planning an impact mission is to calculate the impact energy. Impact energy is calculated using Equation (2).

$$E_i = \frac{1}{2} m_P V_i^2 \tag{2}$$

Using the dry mass of a Star 48B and the approach velocities for select trajectories, Figure 10 displays impact energy as a function of mission time of flight for the target TNOs.

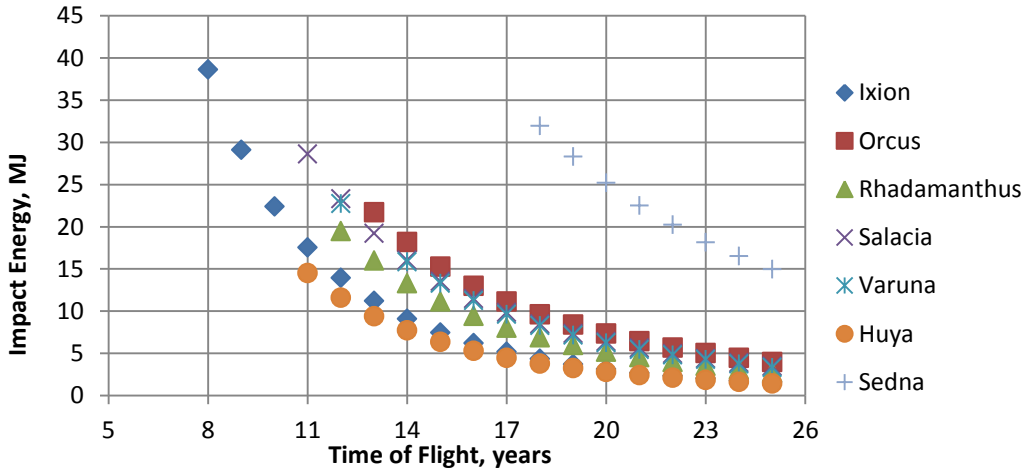

Figure 10. Impact energy vs time of flight. *Impact energy is measured in megajoules, and time of flight is measured in years. The impact mass used to calculate the impact energy is the mass of an empty Star 48B. The impact angle is assumed to be 90°.*

In addition to impact energy, there are several other factors to be considered. The first is the impact angle, which is the angle between a projectile's trajectory and the target's surface. An impact angle of 90° maximizes the impact energy. Maximum impact energy is optimal because the higher the impact energy, the larger the impact crater will be and the larger the debris cloud. This allows for maximum observation and data collection. All of the targets are far enough away from the sun that the spacecraft's orbit should be nearly tangential to the target's orbit. Combined with the fact that all of the TNOs have small gravitational parameters, the spacecraft should have an impact angle of nearly 90° as it approaches the target. An impact angle of 90° was assumed for the data in Fig. 10.

The second factor to be taken into consideration is the position of the observing spacecraft with respect to the impact surface and the sun. The second impactor must follow the same trajectory as the first in order to collect data from the debris cloud. For the best possible viewing conditions, the impact should occur along the terminator as the observing spacecraft passes directly between the impact site and the sun. This situation is outlined visually in Figure 11. However, this position may have to be sacrificed so the flyby spacecraft can observe the crater.

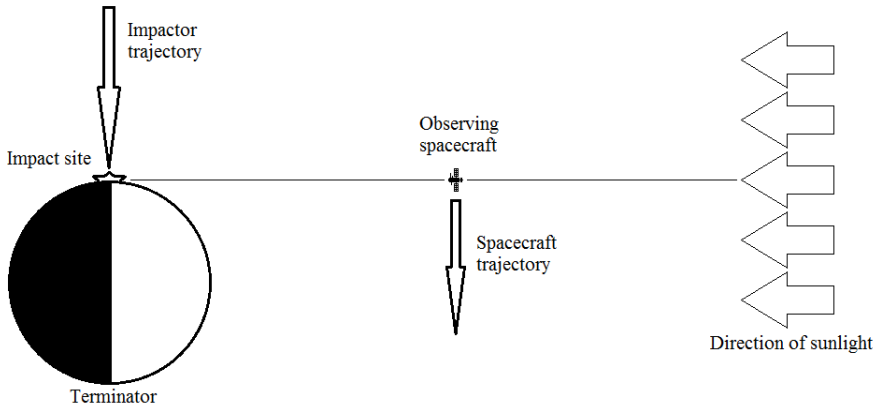

Figure 11. Positions for optimal visual data collection of impact.

A flyby or orbiting spacecraft is best for collecting visual data on the impact. Ideally, this could map the target's surface as well as record the impact. Another important source of potential data collection is the impact crater. Given the impact velocity, projectile mass, and impact energy, knowing the size of the crater allows one to determine the mass and surface density. Thereby, the composition of the target can be better speculated. Since a flyby spacecraft could not pass the target again after impact, an orbiter is ideal for gathering data and images of the crater. An orbiter remains and continues to gather information long after a second impactor or flyby spacecraft. An orbiter can remain with the TNO long enough to observe how and if the debris cloud settles back on the surface, and can also map the target surface more thoroughly than a flyby spacecraft.

The main elements a TNO impact would be aiming to detect are hydrogen, carbon, nitrogen, oxygen, and silicon. Carbon and silicon components are present in spacecraft engine designs, therefore a simple mass of metallic alloys, such as copper and aluminum, would be used as an impactor. This was the method used by Deep Impact. Using an impactor composed of elements foreign to the target allows any reading of those elements to be removed from spectroscopy so they do not interfere with data collection.

Fuel limitations and high ΔV will likely cause the mission to settle for a flyby spacecraft instead of an orbiter. It has not yet been determined which scientific instruments would be most effective for data collection. Either a single instrument that can identify elements or have multiple instruments that identify different elements will be required. If the second case is true, the science payload may need to be adjusted for each TNO based on what results are expected. It also has not yet been determined if the scientific instruments would need to be calibrated in space as the mission approaches its target.

Assuming mass and fuel limitations, the following methodology can be used with two impactors to determine the composition and size of a TNO. While this is not the ideal case and does not allow for surface mapping, vital information can be gleaned. As the impactor approaches the target, it can take a series of photographs. Assuming the size of the TNO, the distance of the impactor from the TNO can be determined. If the impactor also measures time

as it approaches the TNO, it can establish the effect of the TNO's gravitational field on the impactor. From this, a fairly accurate estimation of the gravitational parameter can be found. Combining with the assumed size, this yields a solution for the mass. As the second impactor approaches, it can use a radar or infrared camera to photograph the crater created by the first impact. Using the determined mass of the TNO, the density of the surface can be found based on the size of the crater, which is dependent on the assumed size of the body. Combining the density of the surface with the elements present in the debris, found by flying through the debris cloud, the composition of the surface will be roughly known. Once the composition is known, the next step is to find the albedo based on the composition. From the albedo, you can find the actual size of the TNO from images taken from earth. If this yields a size different than the one assumed, the process can be repeated until a solution converges.

C. Specific TNO Results

Highlighted results for the selected TNO targets are given in Table 4. These represent the ideal launch dates for a given TNO out of the three synodic periods analyzed. As discussed previously, the correlation between low C3, high time of flight, and increased V_∞ can be seen with the 25 and 20 year comparison. For the purpose of orbital insertion, Huya and Ixion have the lowest V_∞ values, and therefore the lowest ΔV requirements. These opportunities occur in 2027 and 2039, respectively. These represent the soonest opportunities to do extensive research on a TNO. This includes being able to insert a payload into orbit with an additional payload for other purposes, such as impacting or flying by.

Table 4. Ideal launch dates for each selected target compared for 25 and 20 year mission duration.

TNO	Launch Date	Time of flight, years	C3, km^2/s^2	V_∞, km/s	R_f, Jovian Radii	Insertable mass, kg
Huya	11/26/2027	25	90.8	3.99	20	384
	11/26/2027	20	92	5.44	17.7	180
Salacia	2/21/2031	25	88.7	7.32	13.8	70.14
	2/22/2031	20	91.86	9.9	9.8	18.8
Varuna	6/6/2022	25	88.2	7	14.22	84
	6/7/2022	20	89.7	9.5	10.2	23.03
Rhadamanthus	9/21/2025	25	94.3	6.5	18.75	84.7
	9/21/2025	20	95.9	8.9	14	20.7
Orcus	7/23/2047	25	88.5	7.5	9.5	63.1
	7/23/2047	20	93.3	10.3	5.4	15.22
Ixion	11/25/2039	25	89.8	4.48	13.7	296.6
	11/25/2039	20	89.26	5.87	13	114.05
Sedna	4/2/2044	25	92.2	14.7	3.3	N/A
	4/4/2044	20	108.9	19.1	1.44	N/A

D. Low Thrust Comparison

Low thrust analysis was done for missions to Huya in order to compare the payload masses inserted into orbit for a maximum 25 year time of flight. The first issue in developing low thrust trajectories was to find a solar electric propulsion code that could be manipulated by undergraduate students with little background in the calculus of variations. Mr. Horsewood, developer of MAnE, also developed a low thrust trajectory code named Heliocentric Interplanetary Low-thrust Optimization Program, HILTOP[8]. This code fit project needs in that it was acceptable for first time users with a limited knowledge of low thrust methods and was used to generate a general analysis of a low thrust mission.

HILTOP supports three optimization parameters for designing missions: maximizing net mass at the primary target, minimizing initial launch mass of the spacecraft from Earth, and minimizing mission duration to the primary target. Analysis was focused on maximizing the net mass at the primary target. In doing so, launch dates were allowed to fluctuate to determine optimal launch criteria for time of flights. Flight durations ranged from 10 to 25 years. HILTOP modeled the launch energy leaving Earth as having a C3 equal to 36 while Earth is in opposition

of Jupiter. Each mission designed had a low thrust portion with powered flight until it reached Jupiter. This powered flight is useful because it lowers the C3 required to leave Earth. This leads to considerably lower values than the C3 of high thrust missions. Having a launch energy as low as one third of a high thrust mission results in a much lighter launch vehicle, which makes for a more cost effective mission. The second leg of every mission constructed consists of a JGA and orbital insertion into Huya's sphere of influence. The second leg of each mission is essentially a ballistic trajectory similar to those in a high thrust mission. The solar panels on the spacecraft are not able to produce the energy needed to run the electric engines at large distances from the Sun due to diminishing engine effectiveness. Therefore, low thrust methods are impractical after the JGA. Since the low thrust engines and solar panels are ineffective at such great distances, the code developed for this project has both of their masses jettisoned from the spacecraft to make for a smaller mass arriving at the TNO and making insertion a more viable possibility.

The spacecraft used for analysis in the low thrust trajectories utilized two NASA Evolutionary Xenon Thruster, NEXT, thrusters[9]. These two thrusters had an input power limit of 14.53 kW. Research found that the NEXT thrusters have efficiency upwards of 70%, but was represented as 65% to account for decay in performance for long duration missions. The NEXT thrusters also have an estimated jet exhaust speed of 37 km/sec. The power required for the spacecraft was modeled as 250 W, the minimal amount of energy needed to keep the spacecraft's engines operating.

It was evident from HILTOP's results that orbital insertion about Huya was possible for a variety of upper stage rockets, heretofore referred to as insertion stages. Information about the insertion stages is listed below in Table 5. The main criterion for an insertion stage was a high specific impulse value. It was later concluded that the insertion stage's dry mass and maximum propellant mass available were also key factors.

Table 5. Insertion Stage Rocket Information.

Rocket Name	I_{sp}, sec	Dry Mass, kg	Max Propellant Mass, kg
Star 63F	297.1	321	4264
Star 37Y	297	81	1070
Star 31	293.5	96.79	1285
Star 48B	292.1	128.3	2009
Star 37XF*	290	66.59	884
Star 48A	289.9	155.1	2429

Analysis of Table 5 shows there is no clear trend for I_{sp} values and their respective masses. Therefore, the code was run with the six different insertion stages listed in Table 5 to see the variations in payload when inserted into orbit about Huya. These trends are shown in Figure 12.

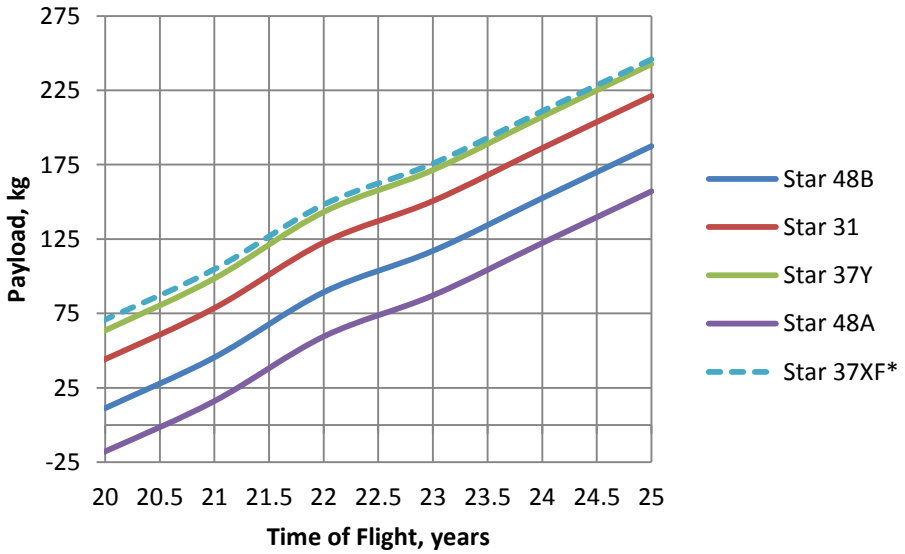

Figure 12. Payload Mass Inserted at Huya for Varying Insertion Stages.

Analysis of Fig. 12 shows there is a strong relationship between flight time and the amount of mass able to be inserted into orbit. This is reasonable since a longer time of flight would result in a lower arrival excess speed as displayed in Figure 3. Figure 12 shows payload inserted into orbit requires a minimum 20 year time of flight. The low C3 value used at launch accounts for most of this.

Figure 13 analyzes the propellant mass. The Star 37XF* exhibited the highest payload masses for insertion, but the amount of required high thrust propellant exceeded the capabilities of the rocket. The same was found for the Star 37Y. The Star 37Y was only able to insert a payload for a 20 and 21 year time of flight before its maximum propellant capabilities were exceeded.

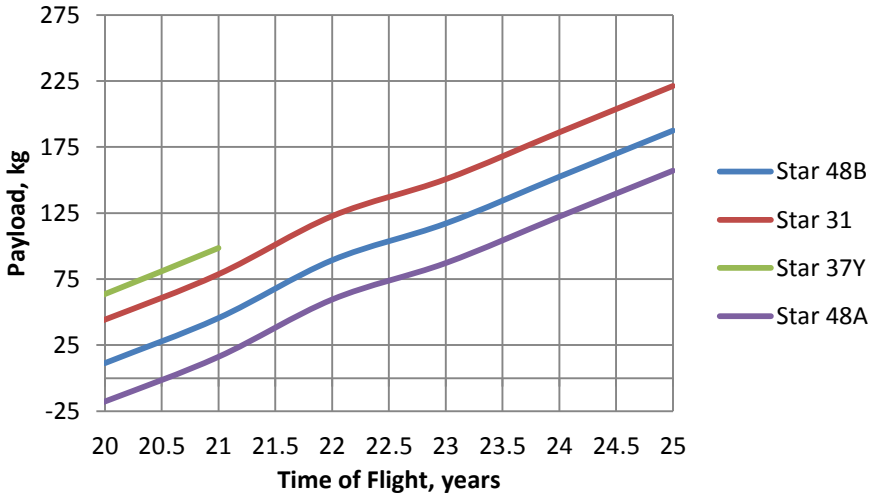

Figure 13. Actual Payload Mass Insertable at Huya for Varying Insertion Stages.

The Star 63F is excluded from both Figures 12 and 13. This is because it does not have the capability to insert a payload for a time of flight range of 25 years, due to its high dry mass weight. However, it seems to have the most promising results for payload inserted into orbit for a time of flight range of 25 to 30 years. A fourth order polynomial fit was put on both Figures 12 and 15 and extrapolated to 30 years. Figure 14 shows the arrival excess speed as a function of time of flight to Huya. This is the same trend that was found for high thrust trajectories. Longer time of flights will always result in a lower arrival excess speed.

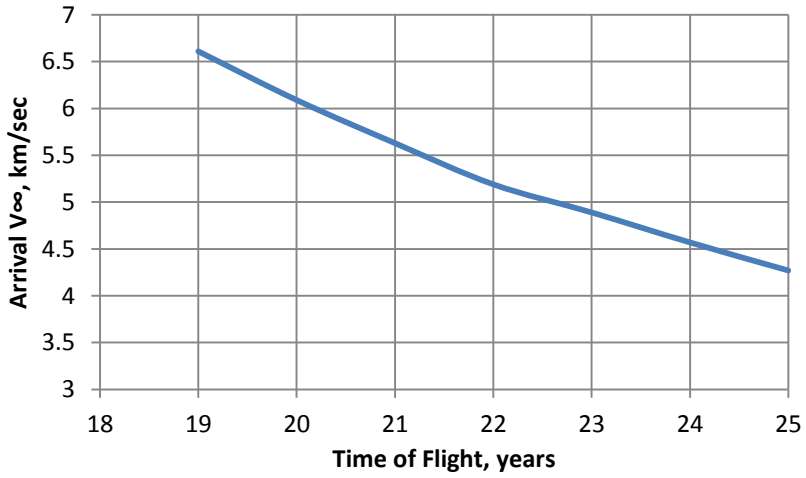

Figure 14. Arrival Excess Speed vs Time of Flight.

The low thrust trajectories developed were originally intended for comparison to a high thrust trajectory using the same configuration. This original comparison was later found to be invalid since none of the high thrust

trajectories found were able to have a payload inserted into orbit about Huya utilizing a single insertion stage. In order to have any comparison made, the optimal payloads inserted into orbit about Huya were compared to the cases produced. Table 6 shows this comparison.

Table 6. Comparison of low thrust to high thrust payloads.

Method	Time of Flight, years	Inserted Mass, kg
High Thrust	25	384
	20	180
Low Thrust	25	221
	20	44

The main discrepancies between the low thrust and high thrust trajectories ultimately result from the launch C3. The high thrust C3s for the 20 and 25 year times of flight are 92 and 90.8, respectively, while both the 20 and 25 year times of flight low thrust trajectories utilize a C3 of 36. This is where the low thrust option can be evaluated as a more viable economic option. The total launch mass of a low thrust mission would be considerably lighter than a high thrust mission since it only requires such a low launch C3. This means a much lighter launch vehicle can be utilized. Additionally, this means there will only be one rocket used for orbital insertion, were as the high thrust cases require multiple rockets.

Figure 15 shows that the high thrust propellant for insertion about Huya is relatively constant for all insertion stages used. It was concluded that insertion stages with higher maximum propellant masses were just as useful as rockets with higher specific impulses. One should note, however, that the high thrust propellant mass requirements go up substantially for increased time of flights. This is a result of the increasing payload masses that can be inserted into orbit as seen in Fig. 12. While the arrival excess speed is lowered for increased time of flights as seen in Figure 14, the mass at the final stage is higher for longer missions. Thus, once at Huya, a larger scientific payload requires more propellant for insertion into orbit.

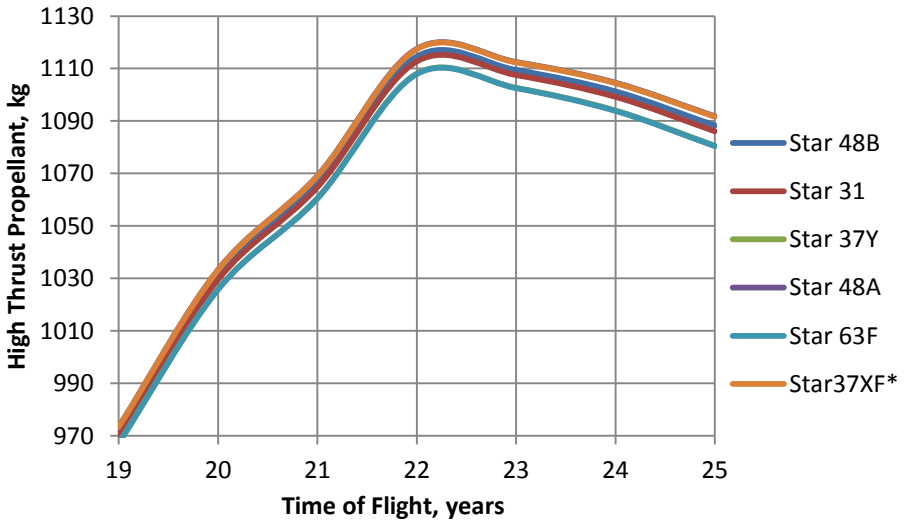

Figure 15. Propellant Needs for Insertion at Huya for Varying Insertion Stages.

Figure 16 is the aforementioned theoretical payload mass that is able to be inserted into orbit at Huya for an extended five year time of flight. The vast increase in payload comes from the much lower excess velocity at arrival and the large amount of propellant the Star 63F has available. This information was gathered by putting a 4^{th} degree polynomial fit on the payload versus time of flight graph for the Star 63F and the propellant mass required for insertion versus time of flight. These two equations were used to extrapolate values for a 25 to 30 year time of flight window. As is seen, these missions seem very advantageous.

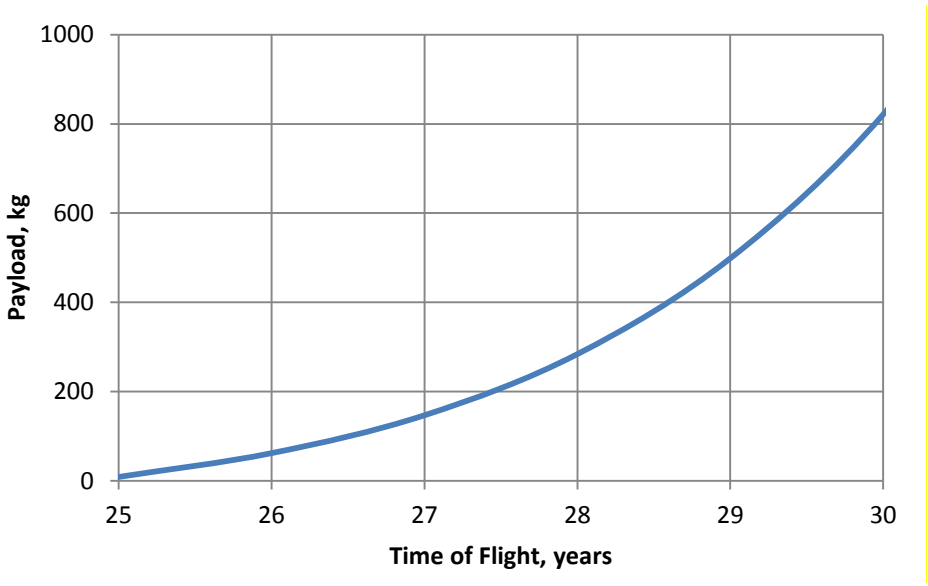

Figure 16. Payload vs Time of Flight to Huya.

Overall, it was concluded that low thrust missions designed to insert a payload into orbit about Huya are feasible for a time of flight window of 20 to 25 years. The range of masses able to be inserted into orbit vary for increasing times of flight and lean more favorably towards the longer times of flight. Multiple insertion stages were explored with the optimal stage for insertion being the Star 31 since its maximum propellant is not exceeded for insertion and it delivers the largest payload to Huya.

IV. Radiation

A well-known concern related to space exploration is the radiation environment in space. Much of the radiation that affects earth operations is produced by the sun, with its intensity related to the distance from the sun, and galactic cosmic radiation, which is very predictable. Another large source of radiation concern for deep space travel is the radiation environment surrounding Jupiter. Since this project used a JGA to assist every mission, this was a factor that needed to be addressed. Historically, Voyager 1 and 2, Pioneer 10 and 11, Ulysses, and New Horizons have all used JGA flybys between about 2 and 33 Jovian radii from Jupiter. The Pioneer spacecraft discovered that the radiation field was much stronger than expected, and gave good reason to study and plan for the environment for future missions.

In the early 1980s, the Jet Propulsion Laboratory at California Institute of Technology, developed a comprehensive model of the Jovian radiation environment. The model was based on the in-situ measurements taken by the Pioneer 10, Pioneer 11, and Voyager missions. The data was updated between 8 and 16 Jupiter radii using data from the Galileo spacecraft mission. To study the radiation from the Jovian system, first the Galileo Interim Radiation Electron, GIRE, Model of the Jovian magnetosphere was obtained[11]. Different methods were then employed to determine the input data needed for GIRE to calculate the radiation distribution on the spacecraft while passing through Jupiter's magnetosphere.

A. Obtaining and Learning GIRE

The code for GIRE was obtained through the Open Channel Foundation. The software package contained two versions of the source code, one of which asks for user input on the Jovian magnetic field, and the other uses an internal magnetic field model. Also included with the source code were sample input and output data files, as well as a report describing the model update, inception, and relevant issues and concerns. Learning how to use the source code proved to be a challenge at first.

The first issue with learning how to use the code stemmed from a lack of experience in the native programming language for the source code, Fortran. Once it was established that the source code could not be properly translated to the MATLAB program language, the next issue arose with obtaining a Fortran compiler. Initially a Fortran 95, F95, compiler was used. However, it was soon determined that GIRE would not work properly on the F95 compiler.

With the help of some collaborators, it was found that GIRE would only work on a F77 compiler, an older version of Fortran.

Having established that the F77 compiler would work, the next issue was to find an F77 compiler. An F77 compiler was found to reside in the University's UNIX accounts. Upon creating accounts and signing into UNIX, it was discovered that UNIX is a fully DOS based system. As with Fortran, this presented a challenge due to unfamiliarity with the system. After learning how the UNIX system worked, the sample input could then be used with GIRE and generate the correct sample output.

B. Compiling Trajectory data

Once a working version of GIRE was achieved, the sample input file was examined in detail. It required eight columns of information. The first three columns were easy to determine, with the headings delta t, RJ, and Latitude. These first three requested the change in time per point in space, the distance from Jupiter in Jovian radii, and the latitude with respect to Jupiter. The other five were difficult to understand and required some research. The headings read: WLNG(SIII), L(VIP4), BSC(VIP4), BEQ(VIP4), and Bcrit(VIP4). Finally, it was determined that these five columns referred to Jupiter's magnetic field.

At this point, trajectory data was needed to attempt to run GIRE. The trajectories generated by MAnE were accompanied by detailed output files, but the specific trajectory data around Jupiter need to run GIRE was not included. To solve this issue, a code was written in MATLAB to find the required trajectory data using some of the outputs from MAnE.

The MATLAB code used orbital mechanics to determine the hyperbolic trajectory the spacecraft would take around Jupiter. In order to use orbital mechanics equations, certain outputs from MAnE were needed. Initially, the outputs required included the hyperbolic excess speed at Jupiter, periapse radius, and turn angle. With these values, the periapse velocity, eccentricity, semi-major axis, semi-minor axis, offset distance, and angular momentum could be calculated. The periaspe velocity was determined using a manipulation of the energy equation given as Equation (3), using μ of Jupiter. Next, the angle between the axis and the asymptote was calculated using Equation (4).

$$V_p = \sqrt{\frac{2\mu}{r_p} + V_\infty^2}, \tag{3}$$

$$\beta = \frac{180-\delta}{2}, \tag{4}$$

Having this angle, the eccentricity of the trajectory could be calculated using Equation (5). Following, the semi-major and semi-minor axes was found using Equations (6) and (7).

$$e = \frac{1}{\cos\beta}, \tag{5}$$

$$a = -\frac{\mu}{V_\infty}. \tag{6}$$

$$b = -a\sqrt{e^2 - 1}. \tag{7}$$

Next, the offset distance would be calculated using Equation (8).

$$B = \frac{r_p V_p}{V_\infty}. \tag{8}$$

Finally, the angular momentum could be determined with the use of

$$H = BV_\infty. \tag{9}$$

With all these values calculated, the next step was to use them to create a visual representation of the trajectory around Jupiter. This was done by initially setting arbitrary large endpoints to be used on the x-axis of the plot, which would later be fine-tuned for a better view of the trajectory. Next, the equation, Eq. (10), for plotting a hyperbola would be used.

$$y = \sqrt{a^2\left(\frac{x^2}{b^2} + 1\right)}, \tag{10}$$

The y value corresponded to the y-axis and the x value to the x-axis of the plot. The values then had to be corrected into Jupiter radii for an easier interpretation of the plot and because GIRE uses Jupiter radii as an input. A unit circle was added to the plot to represent Jupiter at the origin. This meant that the calculated trajectory values had to be corrected to depict an accurate representation of the trajectory going around the representative Jupiter on the plot. With the corrections in place, a model of the trajectory would be displayed and a list of Jupiter radii, in vector form, was given.

Next, the vector values of the radius had to be changed to the magnitude of the radius in order to be used as the input for GIRE. This was done by taking the square root of the sum of the squares. Using the same manipulation that formed Eq. (3), the velocity at each point on the trajectory curve was calculated. After each velocity was determined, initially, the velocity from the first point and the periapse were averaged. Using the vector radii at each point, the total distance of the hyperbola was calculated between the arbitrary endpoints. The time for each point was then calculated by dividing the total distance by the average velocity. This was later corrected since this calculation assumed that each point was an equal time step away from each other, which was not the case. Each point was equidistant from each other. The correction averaged the velocity between each point on the trajectory. The distance between each point was then divided by the average velocity between each point to give an accurate representation of the time for each point.

Having the radius and time now gave two of the three columns needed to be input into GIRE. The next step was to determine the altitude for each of the points on the trajectory. This proved to be a very great challenge. The unfamiliarity with how to obtain latitude data from a planet that is not Earth was great. To remedy this, new outputs from MAnE would be needed and much experimentation with different equations would be used. The new MAnE outputs needed were the inclination, angle of the right ascension, and the angle of the argument of perigee.

The right ascension and argument of perigee were used to determine the point on the trajectory where the spacecraft would cross the Jovian equator. A line was placed on the plot of the trajectory as a graphical reference to where the spacecraft passed through the Jovian equatorial plane. A line was placed perpendicular to the previous line as a reference of where in the trajectory the spacecraft would be at either the highest or lowest latitude, depending on whether the craft started above or below the equatorial plane. The maximum latitude above or below the equator was determined by the inclination angle.

Knowing all this information, a series of test codes were employed to try to accurately represent the orbit in a three-dimensional plot. The main method was to try to create a ground track sinusoidal trajectory as the approximation. To do this, the amplitude of the ground track would be calculated with Equation (11).

$$A = R\sin(i), \tag{11}$$

Next, the frequency for the sine wave was determined through the use of the time it took between when the spacecraft crossed the equatorial plane and when the spacecraft was at the maximum or minimum. With the use of Equation (12), the height above or below the equatorial plane was found using angular frequency and phase shift.

$$z = A\sin(\omega t + \varphi), \tag{12}$$

The phase shift was difficult to determine and was manually manipulated. Through the use of this, one set of data for one of the cases looked like a reasonably close approximation of how the trajectory might actually have looked. However, checking the initial points and endpoints with those recorded in MAnE quickly revealed that it was not as accurate as initially thought.

Unfortunately, this process was very time consuming and the phase shifts were very difficult to calculate, which made calculating correct values for the z variable a long and tedious affair. It was at this point that a decision was made to stop progress on this specific trajectory code. While this code was getting decent results for the two dimensional trajectory, there was a much more powerful code that would give much more accurate results. This code is called the Program to Optimize Simulated Trajectories, POST.

C. POST

When the use of POST was started, it was immediately apparent that this program code was much more powerful than that of the original hyperbolic trajectory code. It took into account many things that the original code did not. One of the main items it took into account was the oblateness of Jupiter. This has a huge effect on how the

spacecraft would actually react to Jupiter's gravitational pull, which would result in a much more accurate trajectory. Initially, the program was set up for use with a flyby around Saturn. This was remedied by collecting the oblateness data for Jupiter from the NASA website, the starting altitude, the equatorial and polar radii, Jupiter's rotation rate, and Jupiter's gravitational constant. The starting altitude used for the different cases was the distance to Jupiter's sphere of influence.

However, many things made the use of this program very challenging. The first challenge was that POST was written to be used in the UNIX accounts. This was a challenge because of the unfamiliarity with editing files within the UNIX account. GIRE did not need to be edited directly, only the input file needed to be, and that could be edited outside of UNIX. The second challenge dealt with debugging the code. While the program was extremely powerful, if something was input incorrectly, the output would show very odd results or would not even work all together. When this was the case, it was difficult to determine the exact cause of the program failure. The use of the manual for troubleshooting proved futile as the manual itself was less user friendly than the program. Another issue was the length of time the program used to give output data. It was generally accepted to let the program run for five minutes and manually stop it to check whether the results were usable.

After a few weeks of changing inputs in POST, running the program, debugging when necessary, and checking results, it was apparent that it was a very slow going process to use POST. Because of the amount of time POST was using, it became apparent that a faster method would have to be used. Looking externally, another code was discovered, which may be able to provide the needed outputs to run GIRE. This code was a MATLAB Jupiter Flyby code developed by a graduate student, Stephen Phillips.

D. Jupiter Flyby Code and Its Modifications

This new code looked very promising since there was much familiarity with the use of MATLAB. Reading through the lines in the code, it became apparent that this code was more powerful than the original hyperbolic trajectory code but not as powerful as POST. This code included a section dealing with the oblateness of Jupiter which was not as comprehensive as POST's but was something that was missing in the original trajectory code. However, like POST and the other trajectory code, this flyby code had many issues.

Originally, the flyby code was asking for the inertial distance from Jupiter, inertial speed, inertial flight path angle, inertial velocity azimuth, latitude, and longitude. Most of these inputs were given by MAnE, such as the inertial speed, distance, and latitude. Longitude was just assumed to be zero initially and the flight path angle and velocity azimuth could be calculated using orbital mechanics. When ran, the Flyby code would result in two plots. The first plot showed distance against time and the second showed latitude against time. These results were those needed to run GIRE.

Since it was a long process calculating the needed variables for use with the Flyby code, it was decided that it would be modified to use the inputs we were already generating from MAnE. The inputs for the Flyby code would be changed to initial distance from Jupiter, initial inertial speed, inclination, initial declination, pass distance in Jovian radii, and initial longitude. Written into the code were calculations for the initial inputs of flight path angle and velocity azimuth based on the current inputs. This would make using the Flyby code a much faster process.

Unfortunately, the resulting plots did not make sense. The first plot would show that the spacecraft would eventually hit Jupiter. It would also show that to go from the sphere of influence distance to about one-fifth of that distance would take roughly 16 minutes. This did not make sense as the spacecraft would have to be travelling much faster than it was in order to accomplish such a feat. The second plot also did not make much sense. It would show that during the same time frame and distance, the craft would only move through tenths or hundredths of degrees. This did not make sense since the inclination angle was much higher for the tested case. This was a turning point to return to POST.

E. Returning to POST and Obtaining GIRE Inputs

It was revealed that the originally used flight path angle was incorrect. The original angle was a positive value, which would mean that the craft would move away from Jupiter. This correlated with the results being received from POST. When the flight path angle was made negative, the results from POST were similar to those from the Hyperbola code. Due to this, it was revealed that POST was getting the results needed for the GIRE inputs. The outputs for POST were changed to include the time step, altitude, velocity, longitude, and latitude.

Using these outputs, a MATLAB code was developed to create a three dimensional plot that showed the true trajectory around Jupiter. The inputs used to generate this plot were the longitude, latitude, and altitude. Since these values are used in a spherical coordinate system, they were converted to Cartesian coordinates to be plotted. This resulted in a plot of the trajectory in three dimensions.

Next, a chart containing data for the other GIRE inputs, those dealing with the magnetosphere, was obtained. This chart was obtained through the NASA website and gave insight on the SIII and VIP4 values. SIII stands for the System-III rotational coordinates of Jupiter. VIP4 stands for the Voyager Io Pioneer 4^{th} order spherical harmonic magnetic field model. The combination of these two values help in determining the vector magnetic field and field line mapping from the Galilean satellites to Jupiter. The fact that VIP4 shows a vector for the magnetic field revealed the reason there were multiple columns needed in the GIRE input file. VIP4 was also found to be valid within 30 Jovian radii. This is good since the resulting periapse radii for each TNO is within this distance.

With all the GIRE inputs accounted for, GIRE could then be used to obtain radiation results. Unfortunately, there was not enough time to complete this. The process of obtaining the needed inputs took entirely too long. Between the back-and-forth use of different programs and codes and being able to generate results that could be used in GIRE, no time was left to actually complete the GIRE calculations and have them interpreted. Sample figures that were generated are in the appendix. Although there are no results for the radiation profile around Jupiter, there are results that will allow future projects to obtain actual radiation data.

V. Conclusion

Every TNO studied can be reached with an optimum launch date within the next fifty years, with many dates falling within twenty years or less. C3 for these missions can easily be kept under 100, with Huya and Ixion being the optimal candidates for an orbital mission. In addition to the missions shown in Table 4, there are many variations and many more dates available for launch depending on the objectives or desired mission length. Acceptable trajectories were found for flight times as low as ten years, with a V_∞ similar to those shown for Sedna in Table 4. The one low thrust comparison made shows that low thrust methods are a viable option for TNO missions and can reduce launch costs. Further comparisons for other TNOs could be made in order to solidify that evaluation. Radiation analysis did not result in conclusive data, but has provided a solid basis for future analysis. While high thrust missions are very possible, low thrust should be researched more for potential cost savings, as well as completing radiation analysis to determine ideal flyby distances for specific missions.

Appendix

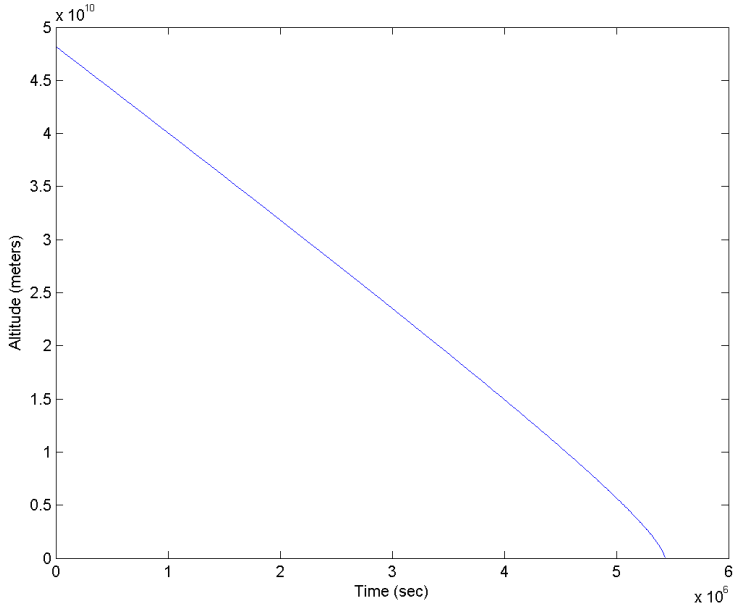

Figure 1. Altitude versus time for Ixion 25 year flight time

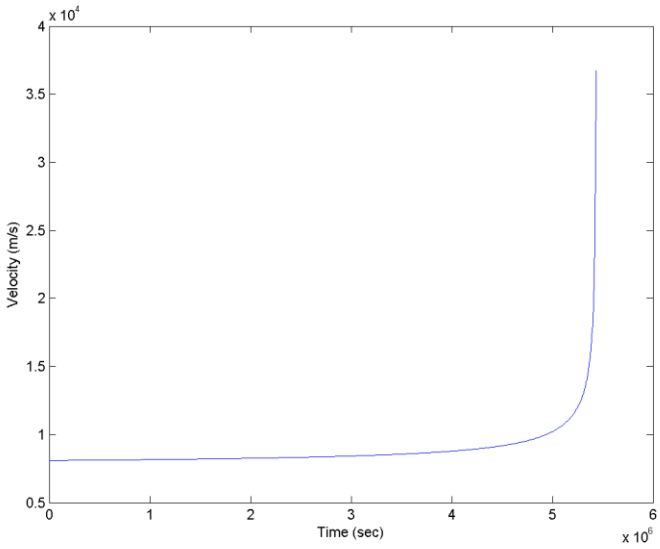

Figure 2. Velocity versus Time for Ixion 25 year flight time

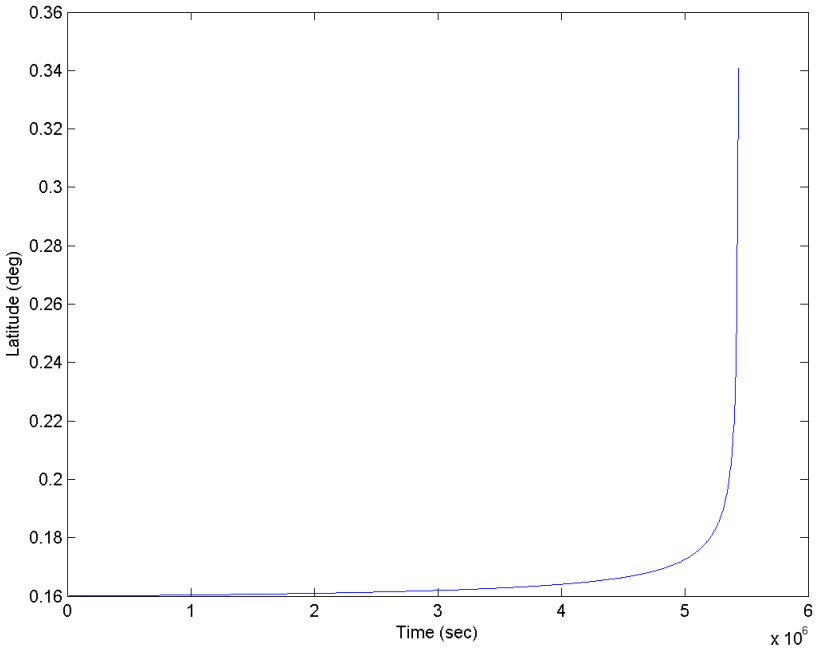

Figure 3. Latitude versus time for Ixion 25 year flight time

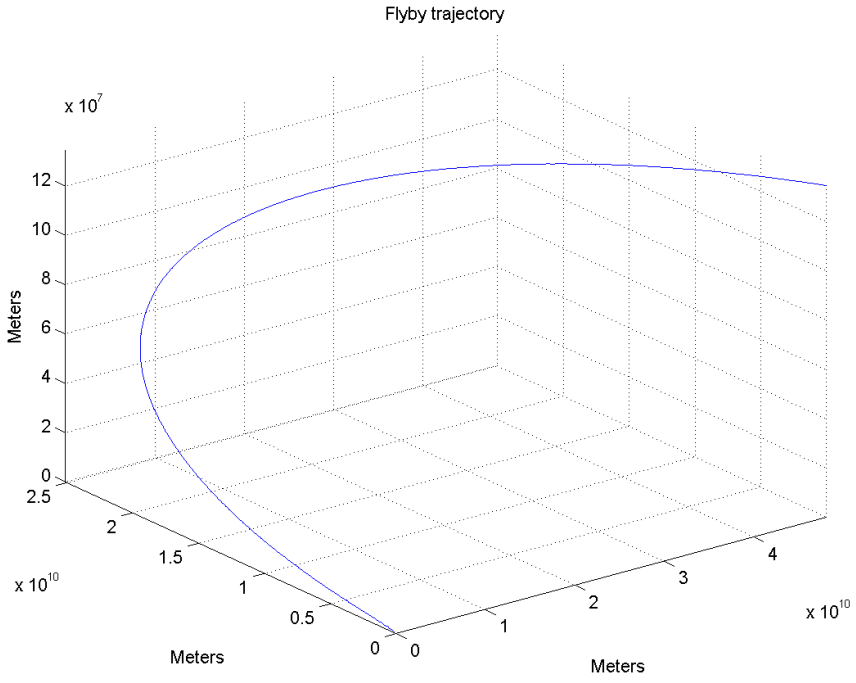

Figure 4. Flyby trajectory for Ixion 25 year flight time

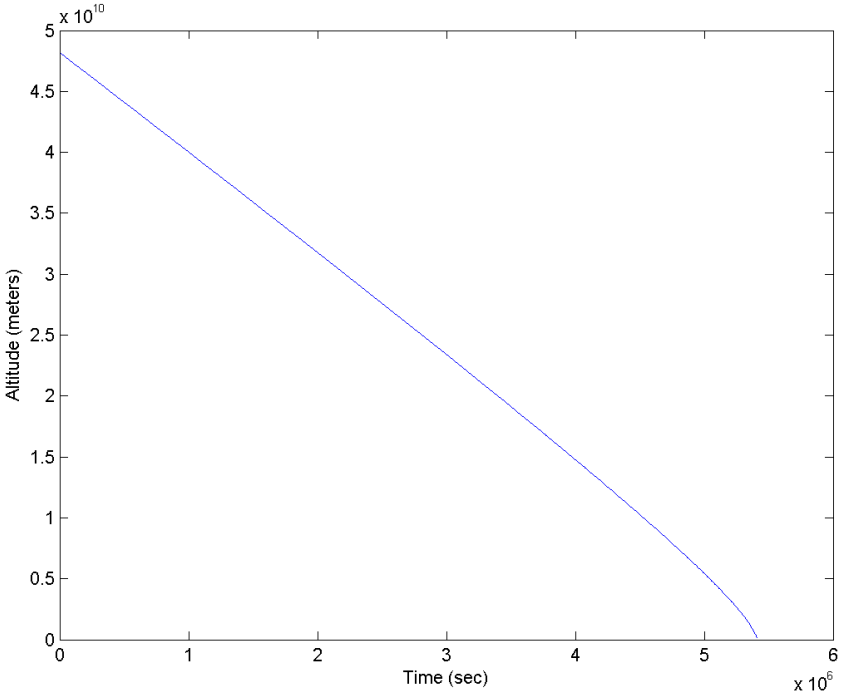

Figure 5. Altitude versus time for Huya 20 year flight time

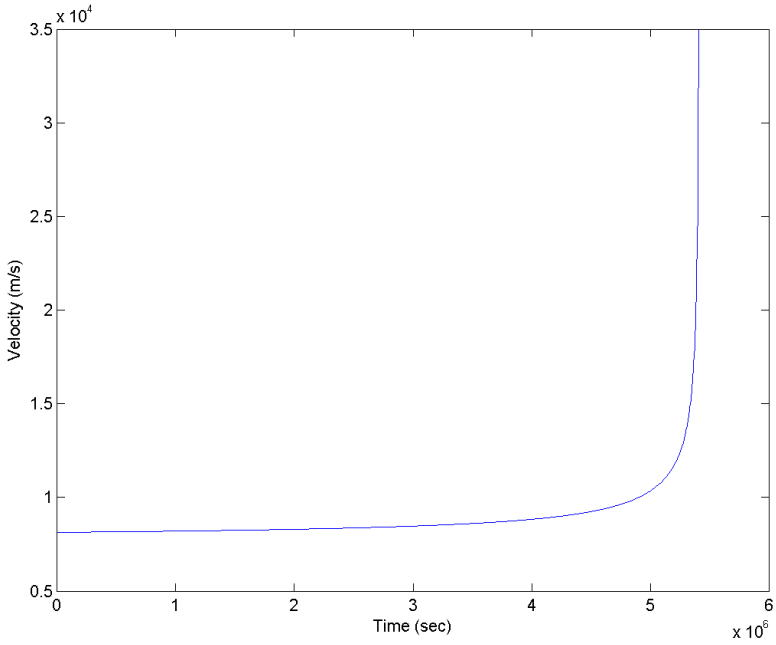

Figure 6. Velocity versus time for Huya 20 year flight time

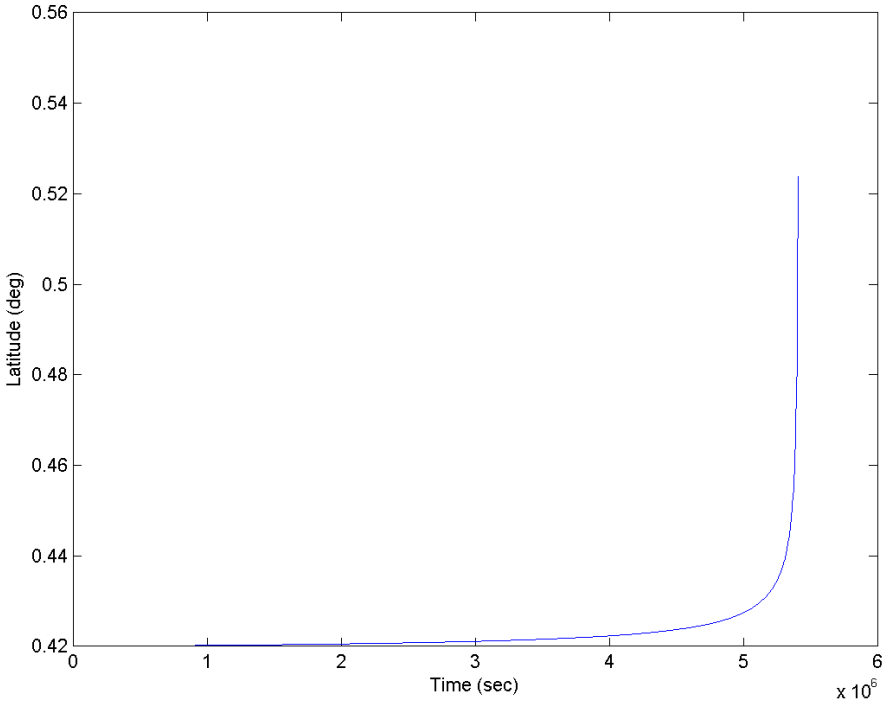

Figure 7. Latitude versus time for Huya 20 year flight time

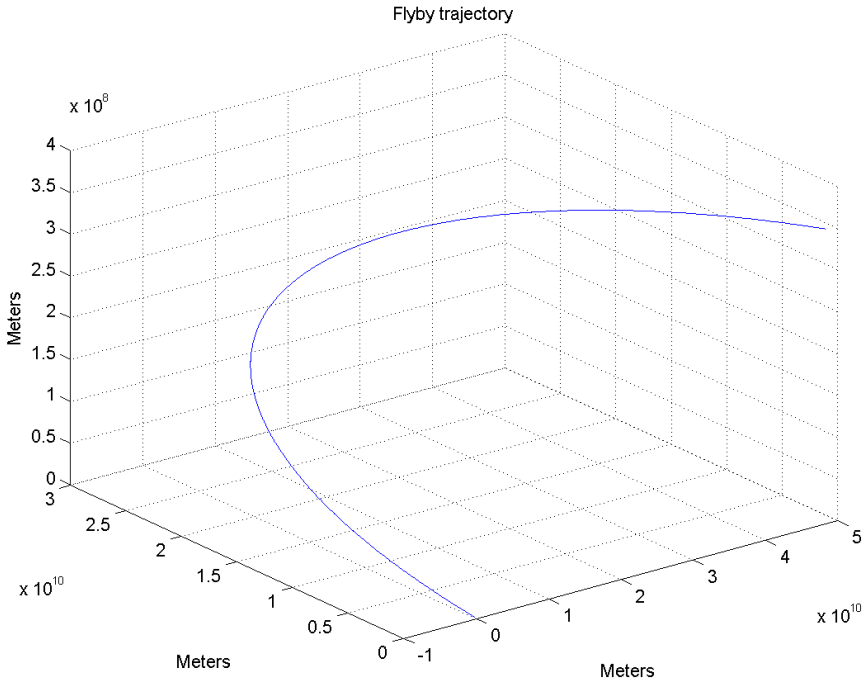

Figure 8. Flyby trajectory for Huya 20 year flight time

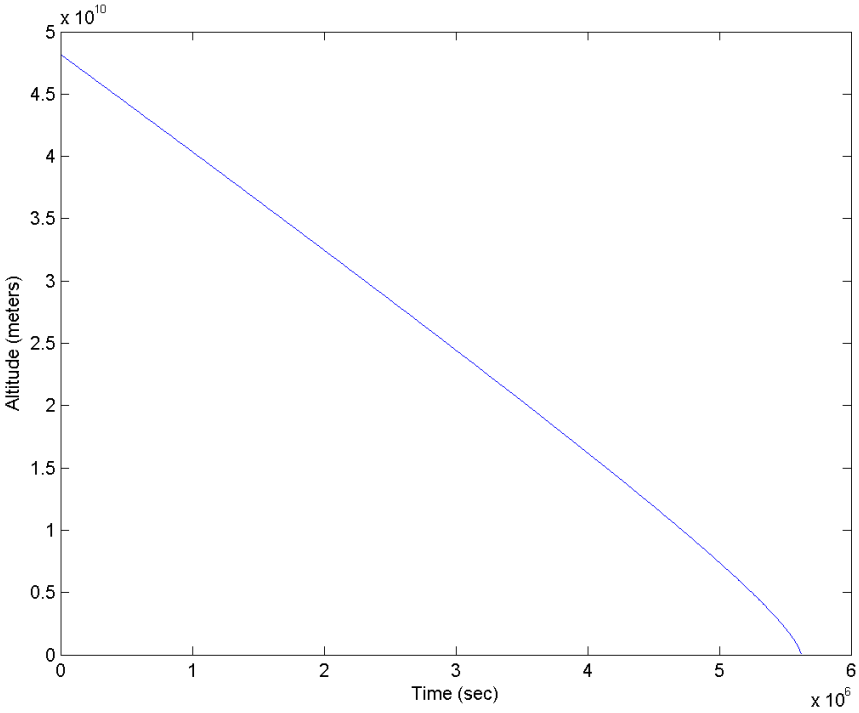

Figure 9. Altitude versus time for Huya 25 year flight time

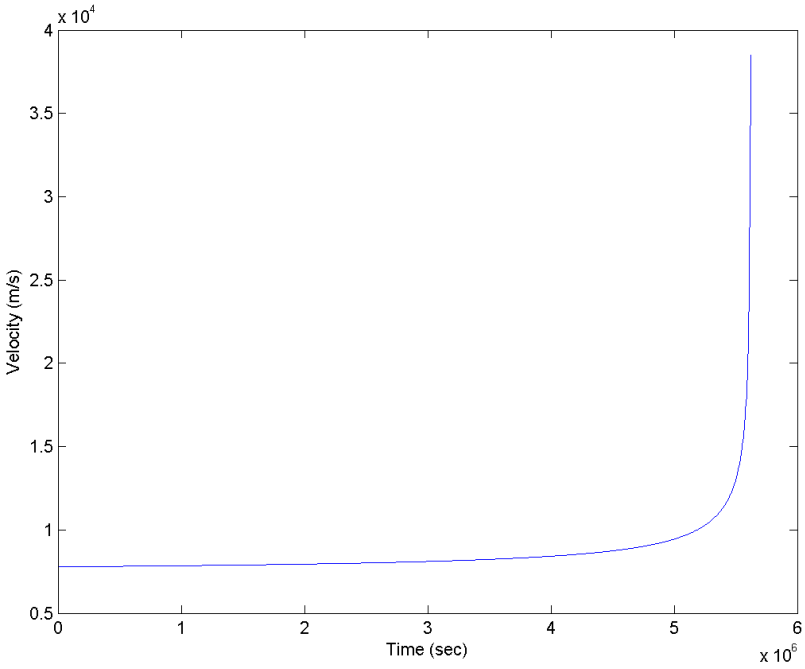

Figure 10. Velocity versus time for Huya 25 year flight time

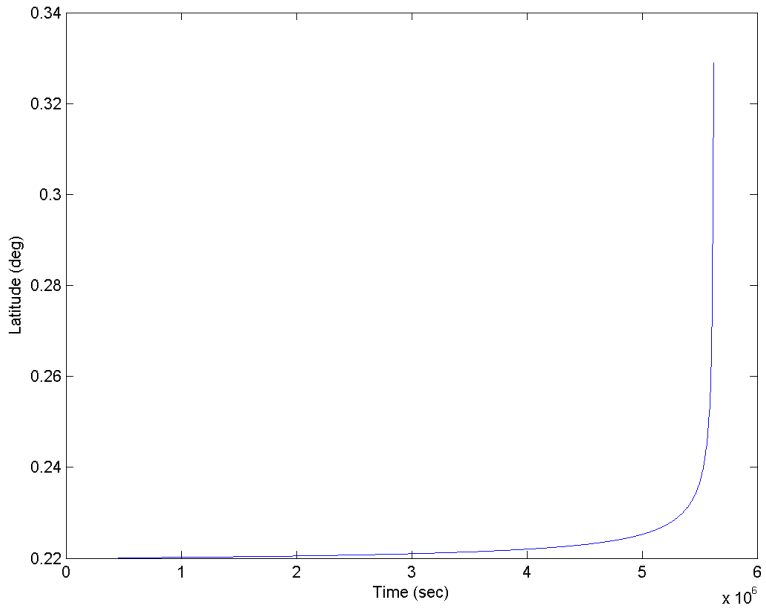

Figure 11. Latitude versus time for Huya 25 year flight time

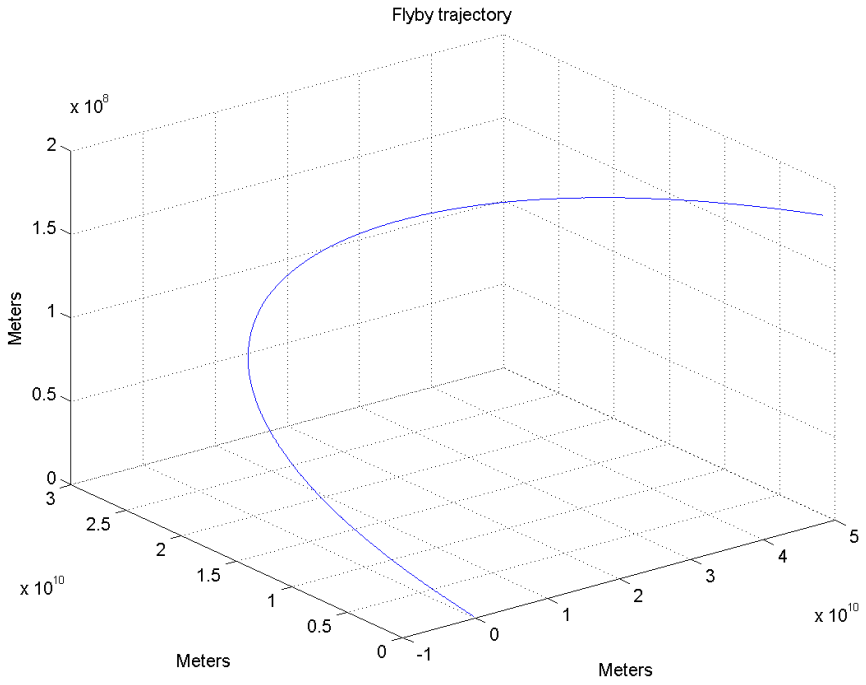

Figure 12. Flyby trajectory for Huya 25 year flight time

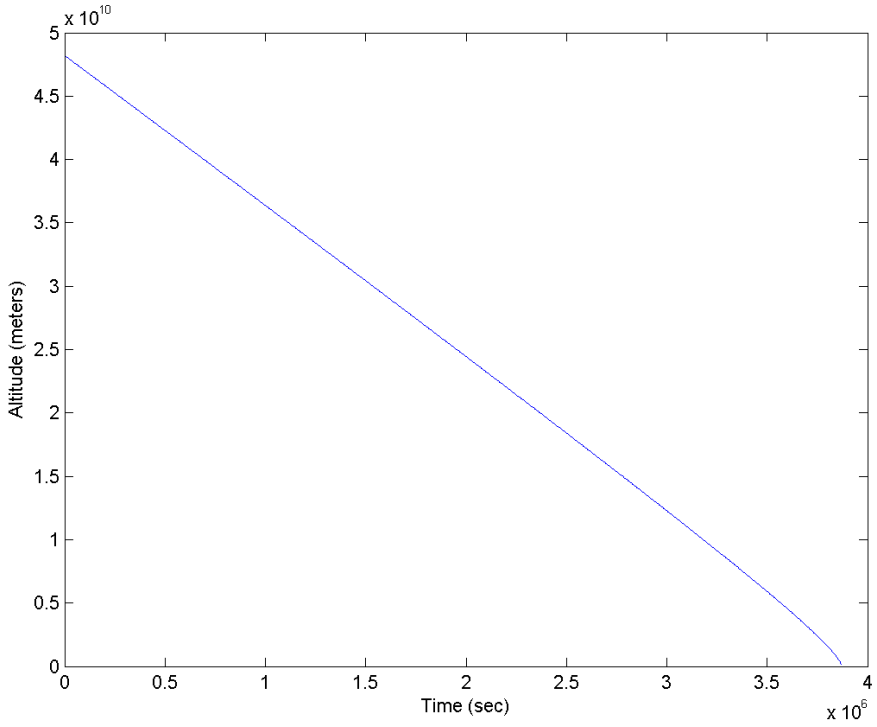

Figure 13. Altitude versus time for Salacia 15 year flight time

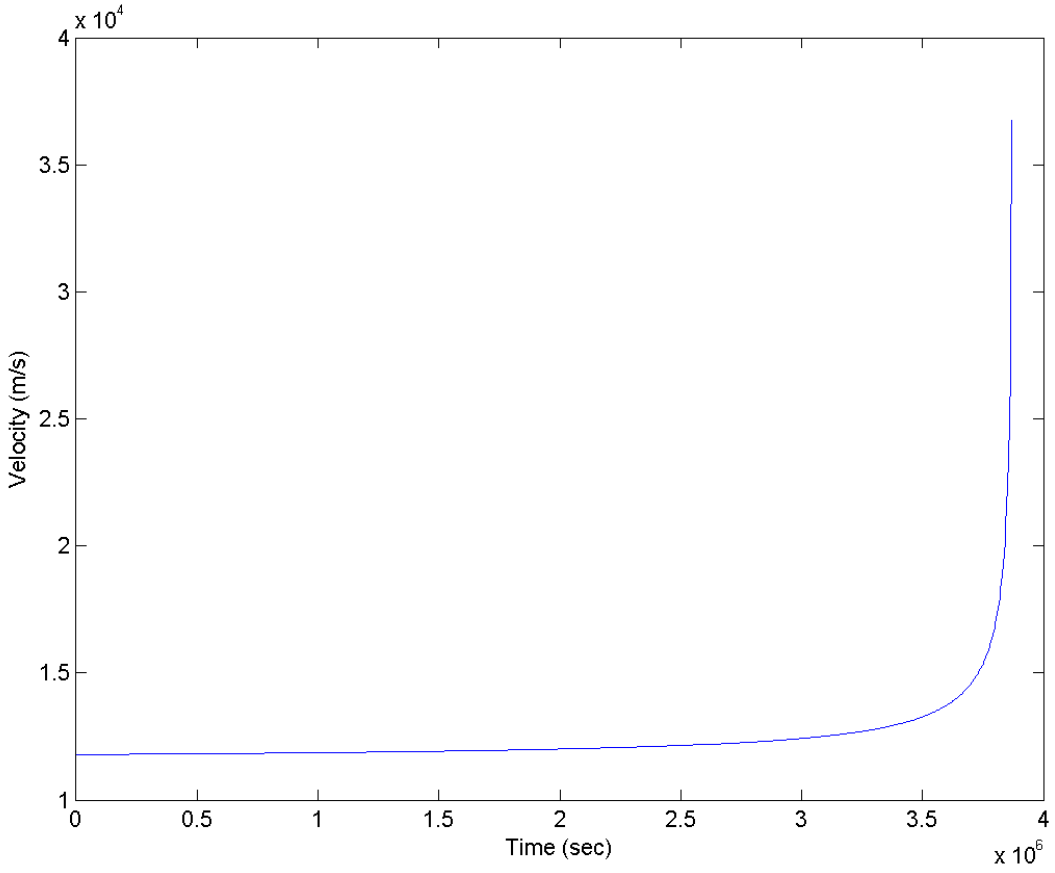

Figure 14. Velocity versus time for Salacia 15 year flight time

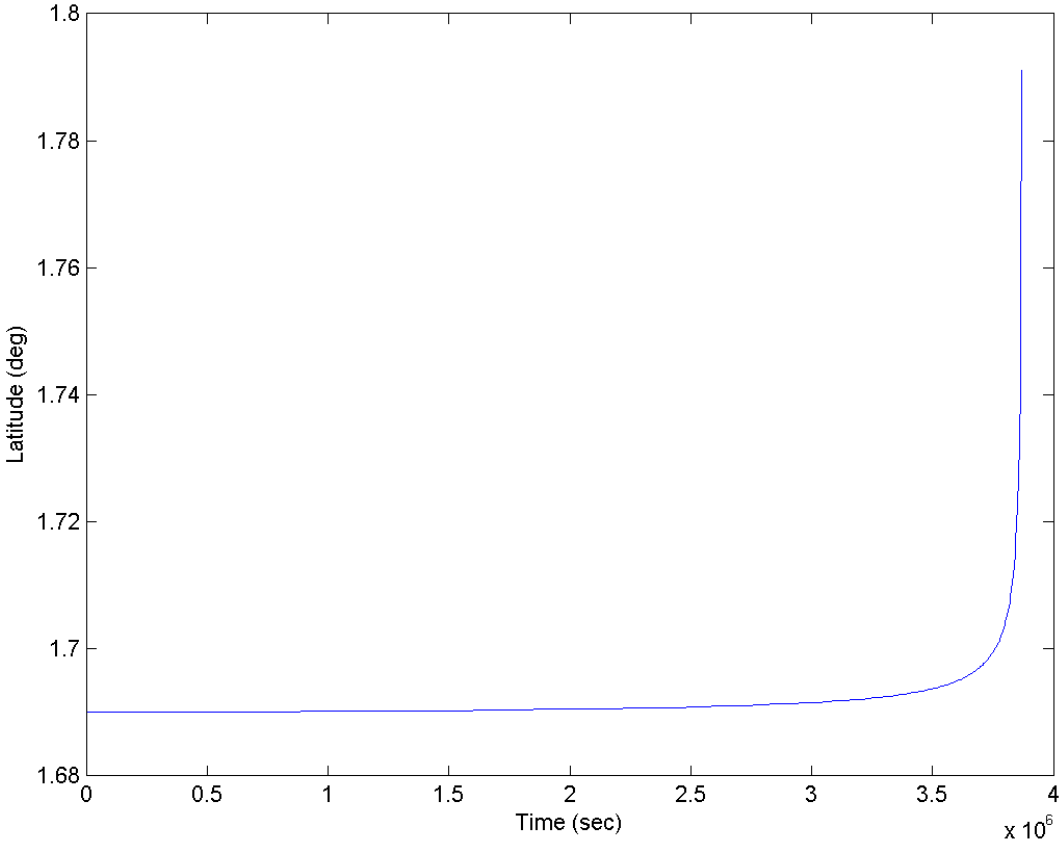

Figure 15. Latitude versus time for Salacia 15 year flight time

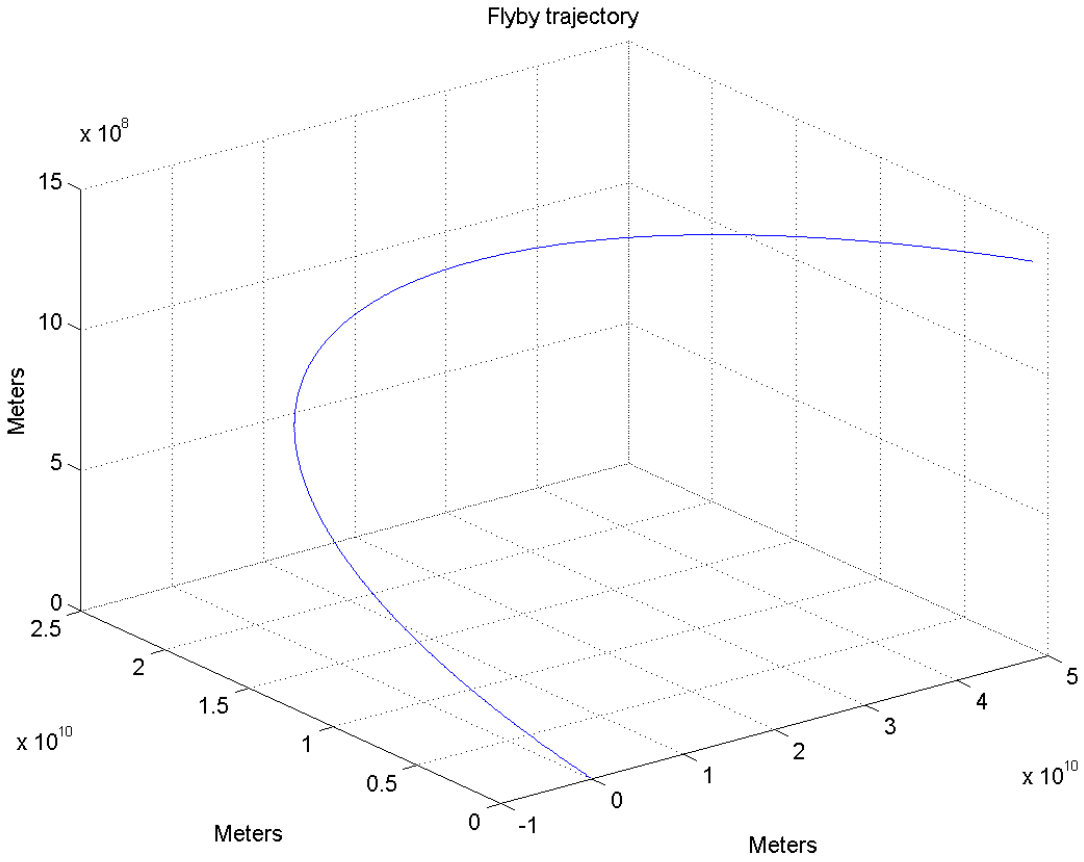

Figure 16. Flyby trajectory for Salacia 15 year flight time

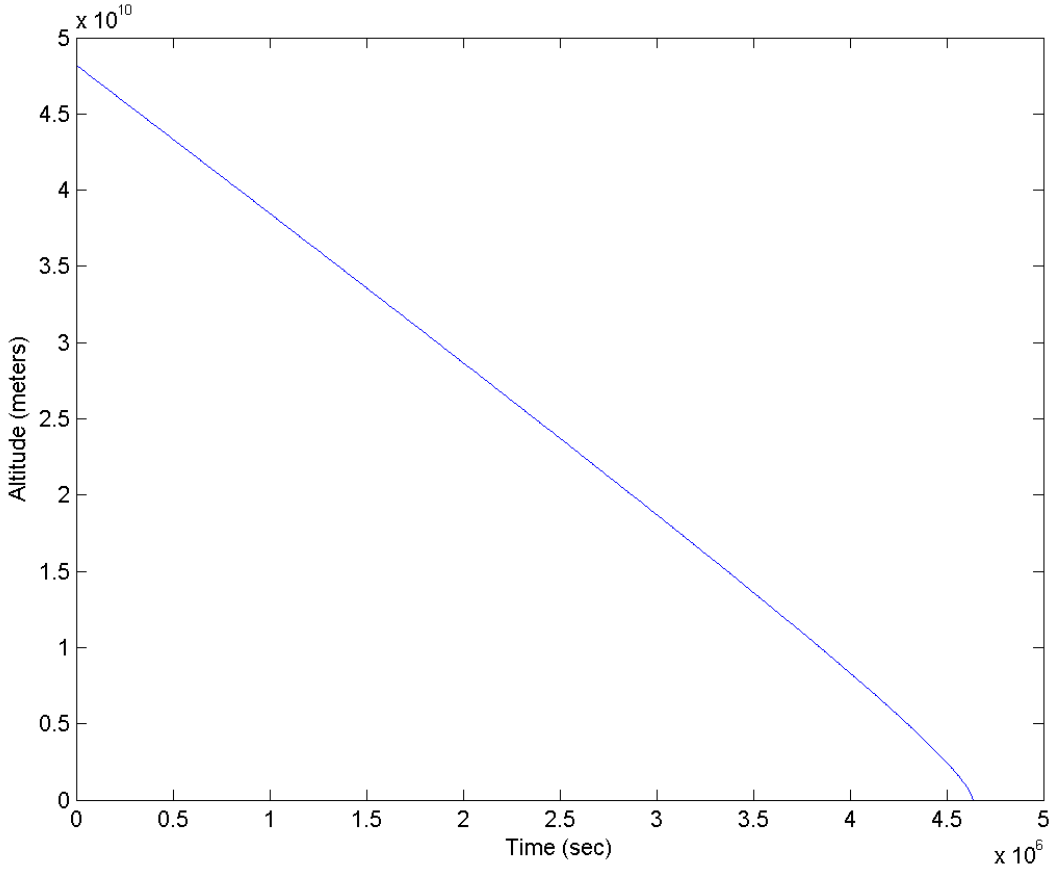

Figure 17. Altitude versus time for Salacia 20 year flight time

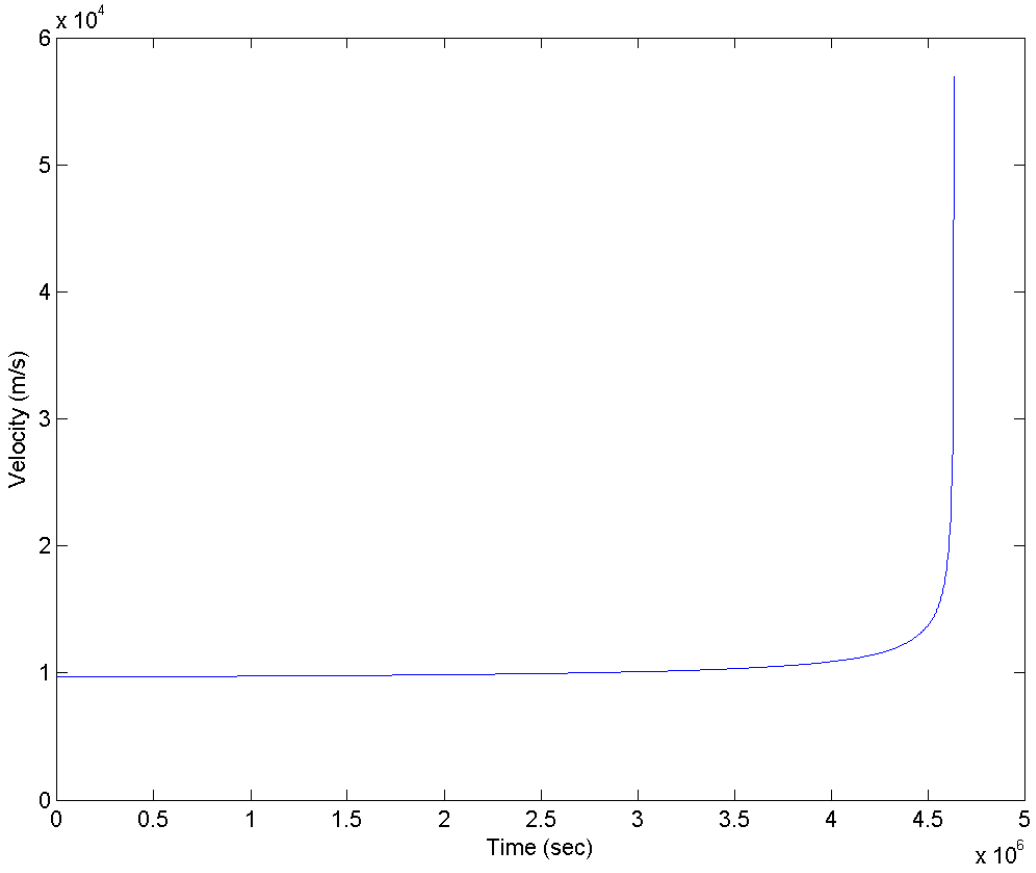

Figure 18. Velocity versus time for Salacia 20 year flight time

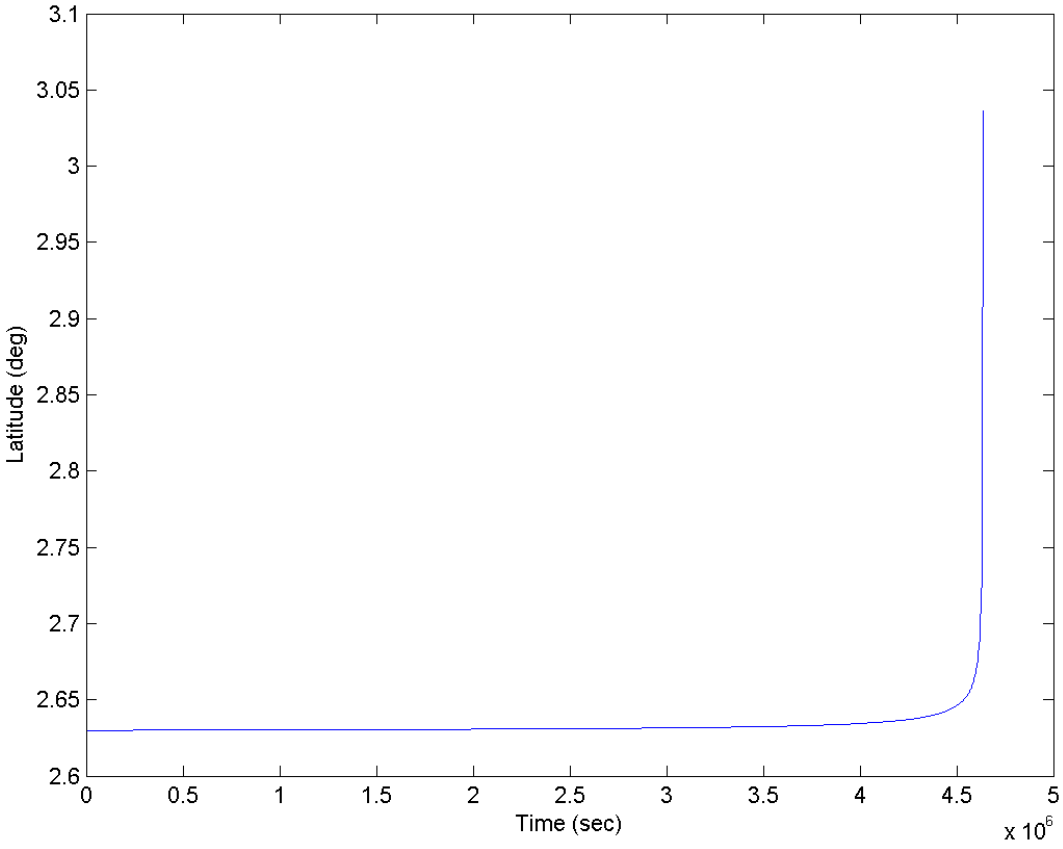

Figure 19. Latitude versus time for Salacia 20 year flight time

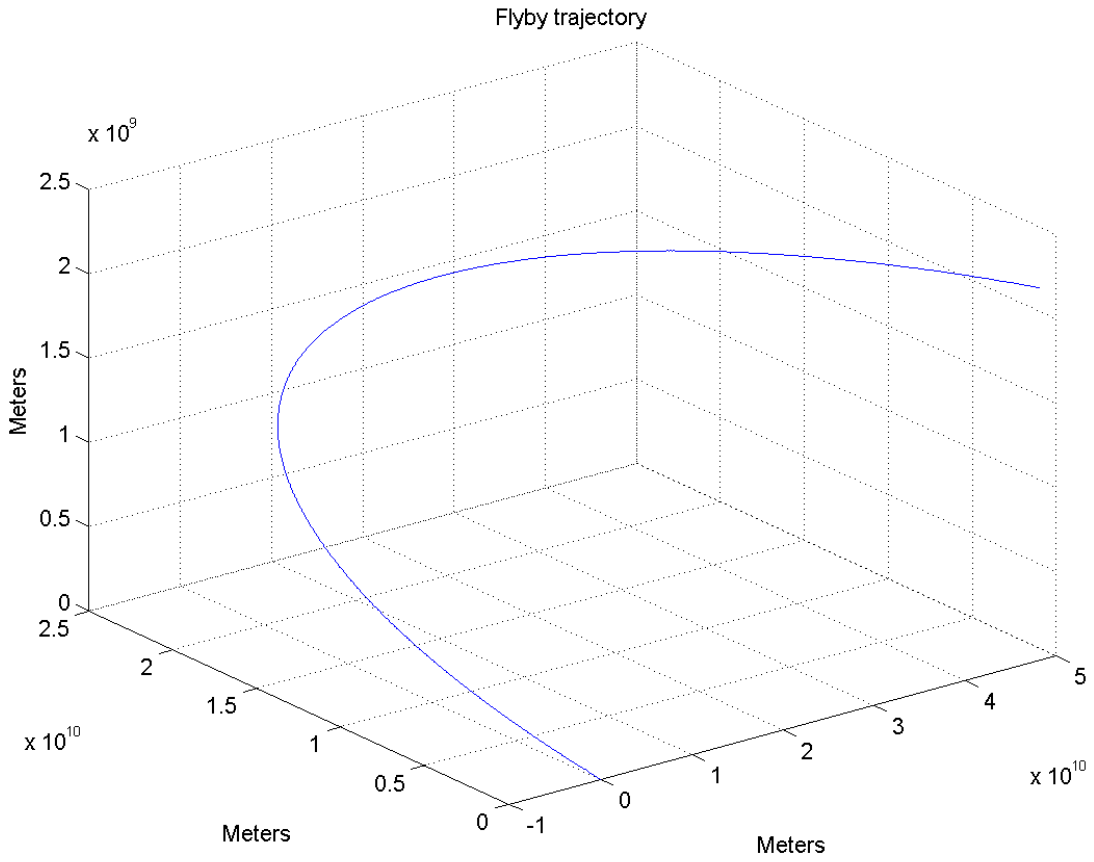

Figure 20. Flyby trajectory for Salacia 20 year flight time

Acknowledgments

We would like to thank Jerry L. Horsewood of Spaceflight Solutions for allowing us to use his trajectory codes, MAnE and HILTOP, which were invaluable to this project.

A.G. would like to thank Ryan M. McGranaghan for his very timely assistance and advice while learning to use MAnE.

A.M. and A.T. would like to thank Mr. Horsewood for his patience in helping us learn how to use HILTOP and for always being available to assist with any technical problems we had.

R.A. and N.Y. would like to thank Dr. Lawrence W. Townsend for his help in troubleshooting the issues we were having while trying to run the GIRE code and for helping us confirm that it could only be used with an F77 version of Fortran. We would like to thank Stephen Phillips for the use of his Jupiter Flyby MATLAB code. We would also like to thank Dr. J. Evans Lyne for providing POST and helping us get it to run.

References

[1] McGranaghan, R., Sagan, B., Dove, G., Tullos, A., Lyne, J.E., Emery, J.P., "A Survey of Mission Opportunities to Trans-Neptunian Objects," *Advances in the Astronautical Sciences Series*, CP11-615, Vol.142, Univelt, San Diego, CA, 2012

[2]Committee on Science Opportunities Enabled by NASA's Constellation System, National Research Board, *Launching Science: Science Opportunities Provided by NASA's Constellation System* Washington, D.C., National Academies Press, 2009, pp. 109.

[3]NASA, *New Horizons, The First Mission to Pluto and the Kuiper Belt: Exploring Frontier Worlds*, Launch Press Kit, 15 December 2005.

[4]Mission Analysis Environment (MAnE), Version 3.5, developed by Space Flight Solutions, Hendersonville, NC.

[5]Celestia, Version 1.6.1, developed by Celestia Development Team, http://www.shatters.net/celestia/index.html, accessed October 2011.

[6]Quigley, N., Allen, R., Gleaves, A., Moon, A., Roe, E., Spencer, D., Tupis, A., "D. Lyne's Guide to the Galaxy", Senior Design Project, Mechanical, Aerospace and Biomedical Dept., Univ. of Tennessee, Knoxville, TN, 2012

[7]Alliant Techsystems Inc., *ATK Space Propulsion Product Catalogue*, May 2008, pp. 40-79.

[8]Heliocentric Interplanetary Low-thrust Trajectory Optimization Program (HILTOP), developed by Space Flight Solutions, Hendersonville, NC.

[9]United States. National Aeronautics and Space Administration. *NASA's Evolutionary Xenon Thruster*. 2008. Web.

[10]Zona, Kathleen. United States. National Aeronautics and Space Administration. *Ion Propulsion*. 2008. Web. <http://www.nasa.gov/centers/glenn/about/fs21grc.html>.

[11]Galileo Interim Radiation Electron (GIRE), developed by NASA Jet Propulsion Laboratory and California Institute of Technology, Pasadena, CA.